Doctoral Dissertation (Shinshu University)

Studies on Dye Cation Reduction and Charge Recombination Kinetics in Dye-Sensitized TiO_2 Solar Cells

March 2015

Junichi Ogawa

Contents

Chapter 1

Introduction

Chapter 1. Introduction

1-1. Renewable energy

Fossil fuels are the world's main energy sources. Excess consumption of the carbon cycle depletes these resources [1]. To avoid depletion, nuclear power generation has been introduced in Japan and around the globe [1, 2]. The nuclear power sources emit little CO_2. However, the fuel source is uranium, which also depletes exhaustible resources. Moreover, the following can be suggested as matters of concern for nuclear power generation. In 1999, the Tokaimura nuclear accident indicated the harmful repercussions of the radiation from the fuel for humans. In 2011, the Fukushima Daiichi nuclear disaster resulted in widespread and long-term damage. Thus, renewable energy sources that are safe and low cost from construction to disposal are desired for a sustainable society. To achieve a sustainable society, renewable energy sources, such as wind-, tidal-, geothermal-, solar-, and hydropower, have been introduced. To harvest such power efficiently, power generation using renewable energy should be introduced appropriately in view of local features.

The development and introduction of solar cell technology could be a solution to the energy crisis. Solar cells are natural and highly versatile energy harvesters capable of generating power anywhere sunlight is available. These cells also have high maintainability due to their low-cost construction materials. There are many types of cells that operate using different energy

conversion mechanisms and constituent materials. These solar cells are broadly classified in two categories based on their charge separation material—inorganic and organic. The inorganic solar cells typically require an expensive vacuum conditioned process, whereas, by contrast, the organic solar cells can be fabricated using an affordable roll-to-roll process under the atmosphere. This process can easily be scaled up. Thus, organic solar cell construction and development has the potential to be a more affordable option. Organic photovoltaics, dye-sensitized solar cells, and perovskite solar cells utilize organic materials.

In this thesis, I focused on dye-sensitized solar cells (DSSCs). The reasons I chose the DSSCs is related to several of their characteristics. The quantum conversion efficiency of DSSCs between the absorbed photons and produced electrons is close to 100%[3]. DSSCs have an excellent design, as they can be colorful and flexible [4, 5]. Therefore, I studied electron transfer kinetics at the interfaces in DSSCs to obtain high power conversion efficiency (PCE).

1-2. History of dye-sensitized solar cells

Transparent metal oxide semiconductors, such as TiO_2, absorb ultraviolet light due to their wide band gaps between the conduction and valence bands. Therefore, PCE is low when there are employed for solar cells because visible light, which takes up most of the solar energy, are not absorbed. When the dye adsorbs on the oxide semiconductor surface, the absorption wavelength region of the electrodes can be extended to the dye-absorption wavelength region,

thereby improving the light harvesting efficiency. However, the absorbance at each wavelength of the dye-adsorbed semiconductor electrodes is low. This low absorbance is derived from the dyes' low molar extinction coefficient. The majority of the visible light passes through the photo-electrode, and thus the PCE is low. In 1976, Tubomura et al. produced a dye-adsorbed mesoporous ZnO electrode cell, which was a prototype of DSSCs showing high photocurrents at 532 nm [6]. The high photocurrents were achieved as a result of the increasing amount of the adsorbed dyes. The increase was due to the large surface area of the semiconductor electrode.

In 1991, Grätzel developed DSSCs using TiO_2 with a ruthenium complex dye that reached 7.1%[7]. This high-energy conversion efficiency of DSSCs was due to the high absorbance of the photo-electrode to large surface areas derived from mesoporous titanium dioxide. This attractive finding resulted in active developments of DSSCs in many parts of the world. In 1993, DSSC using a ruthenium complex dye, N3, achieved 10% efficiency, comparable to the amorphous silicon solar cells[8]. For further performance improvement, multifaceted research using new sensitizing dyes, semiconductor electrodes, electrolytes, and counter electrodes has been done, in addition to electron transfer mechanism investigations and device manufacturing method improvements[4]. In 2005, the PCE reached 11.2% through DSSCs using a ruthenium complex dye N719[9]. In 2006, 11.1% was reported in DSSCs using a ruthenium complex dye N749[10]. After that, significant improvement was not observed, and, in 2010, the conversion efficiency remained at 11% in DSSCs using porphyrin-based YD-2 dye[11].

In 2011, by replacing iodide/triiodide redox couple with cobalt (II/III) complex redox couple, a more than 1 V open circuit voltage (V_{oc}) was reported. This report indicated that the V_{oc} can be increased using cobalt complex redox couples[12]. Combination of a porphyrin dye and a cobalt complex redox couple then showed 12.3% conversion efficiency[13]. The best conversion efficiency to date is 13.0%, which was achieved with SM315 porphyrin dye and cobalt complex redox couple in 2014[14]. Figure 1-1 shows chemical structures of the dyes that DSSCs with the dyes had been achieved the highest power conversion efficiency, and cobalt complex as used for redox couples in DSSCs.

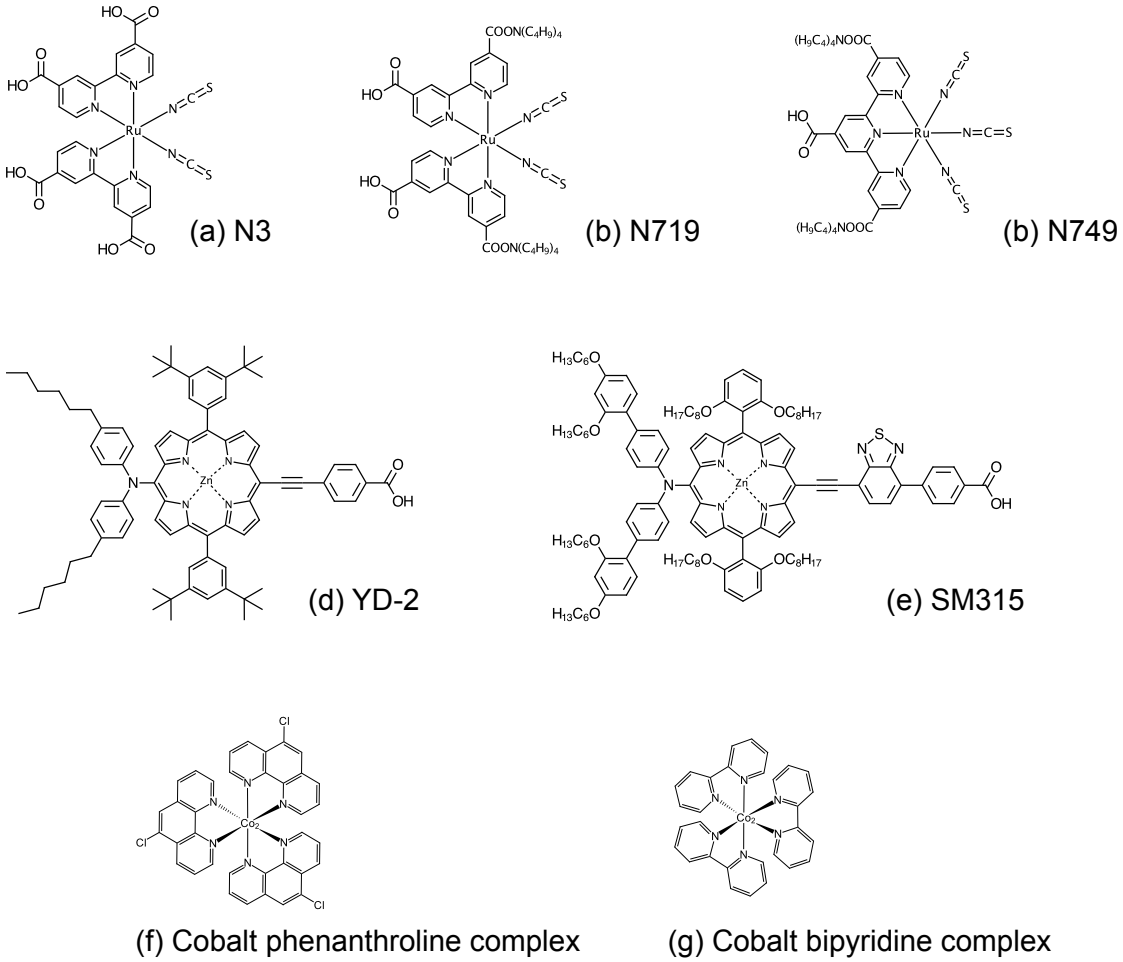

Figure 1-1. (a–e) Chemical structures of dyes. DSSCs using the dyes had been achieved highest power conversion efficiency. Ruthenium complex dye N3[8] (a), N719[9] (b) and N749[10] (c). Zinc porphyrin dye YD-2[11] (d) and SM315[14] (e). (f) Chemical structure of a cobalt complex as used for redox couples in DSSCs that the open circuit voltage was more than 1 V in literature 12. (g) Chemical structure of a cobalt complex as used for redox couples in DSSCs with SM315 in literature 14.

High PCE-marked devices been employed metal complex dyes. Especially, DSSCs using ruthenium complex dyes have a disadvantage due to the costly rare metal. On the other

hand, organic dyes are also being studied. A D-π-A type organic dye is consisted of a donor property organic substituent combined with an acceptor property organic substituent by π-conjugated linker. Schematic representation of the D-π-A structure is shown in Figure 1-2.

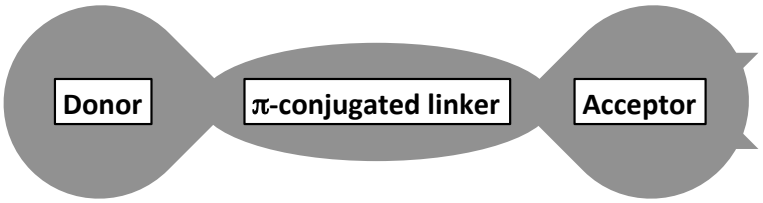

Figure 1-2. Schematic D-π-A type organic dye structure. Each unit is linked via a π-conjugated linker. A typical acceptor unit has a carboxyl group for chemical adsorption to the semiconductor surface.

DSSCs using the D-π-A structured organic dye have the potential to achieve high performance. Since DSSCs require high charge separation efficiency to gain a large current, molecular orbital of lowest unoccupied molecular orbital, LUMO, should be expanded onto the anchoring side to inject the electron from the dye efficiently. On the other hand, the molecular orbital of highest occupied molecular orbital, HOMO, should be distanced from the semiconductor surface to avoid charge recombination between an oxidized dye and the injected electron. The D-π-A structured organic dye successfully obtained the required molecular orbital condition[1518]. In one instance, Figure 1-3 shows the molecular orbitals of the D-π-A structured

organic dye (MK-3[19]) and the molecular orbitals of LUMO and HOMO calculated with DFT on a B3LYP/6-31G(d). Furthermore, the D-π-A structure can extend an absorption wavelength region by an extension of the π-conjugation [15, 20]. Additionally, the D-π-A structured dye can be modified easily and the open circuit voltage can be improved by replacing of donor unit and modifying the substituents [21, 22]. In fact, the DSSCs using D-π-A structured dyes have been recorded as having a high PCE of around 10%[23–25] and that more than 10%[18].

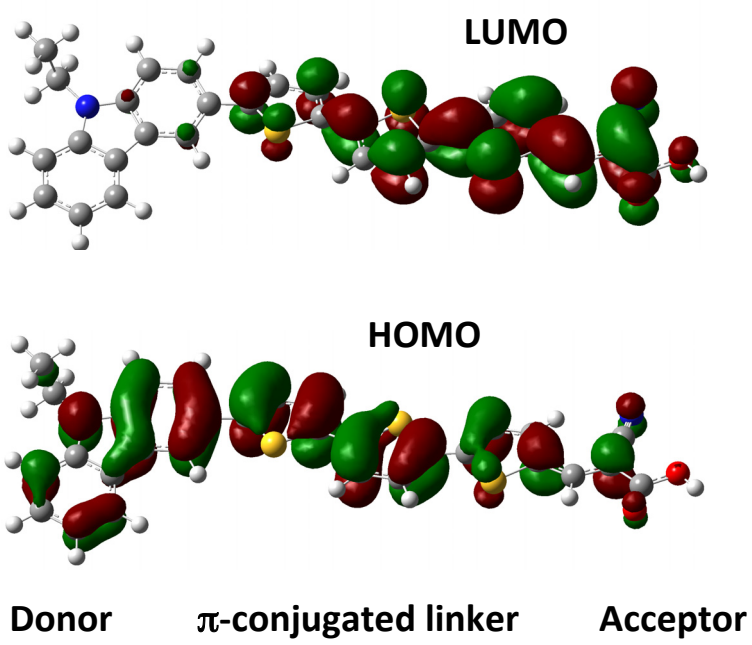

Figure 1-3. Molecular structure of the D-π-A structured organic dye (MK-3) and the molecular orbitals of LUMO (top) and HOMO (bottom). The orbitals were calculated with DFT on a B3LYP/6-31G(d).

1-3. Structure of DSSCs

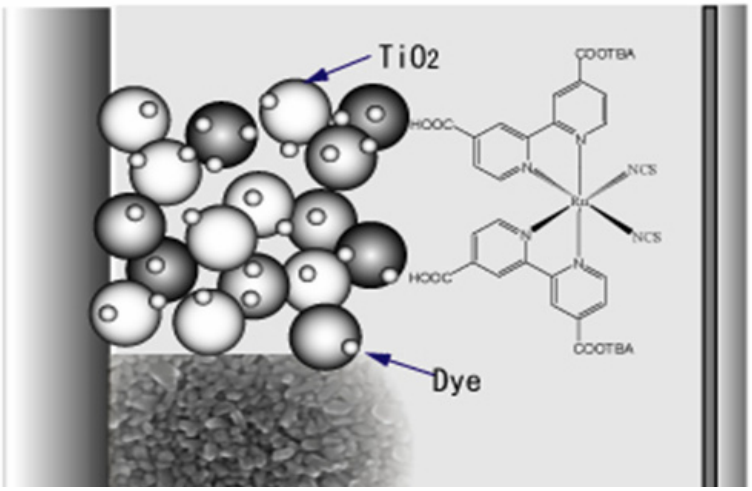

Figure 1-4. Typical structure of a DSSC. The structural formula in the figure is for ruthenium complex dye N719. The semiconductor electrode is composed of semiconductor nano-particles.

Typical DSSCs are sandwiched between a photo-electrode, which is composed of a dye-adsorbed mesoporous semiconductor electrode sintered onto fluorine-doped tin oxide (FTO) glass, and a platinum counter electrode. An electrolyte containing a redox couple is filled between the electrodes (Figure 1-4). I^-/I_3^- is often used as the redox couple.

1-4. Working principle of DSSCs

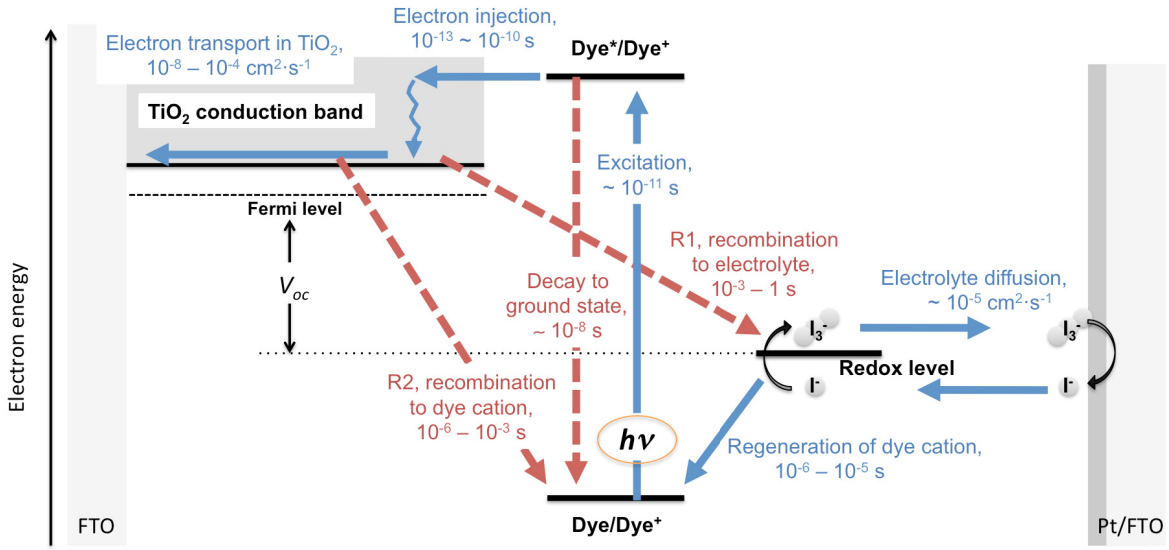

Figure 1-5. Electron transfer kinetics in a DSSC. The solid line arrows indicate electron transfer; broken line arrows indicate electron recombination. When the dye absorbs a photon, ultrafast injection occurs. The injected electron is extracted to an external circuit. A dye cation is reduced by I^-. I_3^- is reduced at the counter electrode. R1 denotes the electron recombination from the conduction band to I_3^-. R2 denotes the electron recombination from the conduction band to the dye cation.

Figure 1-5 shows electron transfer kinetics in a DSSC. The operation of the DSSCs begins by photoirradiation-induced electron injection into the conduction band of the semiconductor electrode. The injected electrons then travel to the FTO by diffusion and then provide work in an external circuit. The oxidized dye due to electron injection, that is, the dye-cation, is reduced by I^-, which is a reactant in the electrolyte, thereby generating I_3^-. I_3^- moves by diffusion to the counter electrode and is reduced, thus completing the electrical circuit

(Figure 1-5). A DSSC operates as a solar cell via a series of electron transfer reactions. Electron transfers in the DSSCs involve not only such ideal electron transfers but also electron recombination. The broken line arrows in Figure 1-5 indicate electron recombination. R1 denotes electron recombination from the conduction band to I_3^-. R2 denotes electron recombination from the conduction band to the dye-cation.

The electron transfer kinetics is not only a required kinetics for current generation, but also competitive charge recombination kinetics in the DSSCs [4]. The charge recombination kinetics is shown as broken line arrows in Figure 1-5. Each of the kinetics was measured in DSSCs using typical constituent materials that materials are TiO_2, ruthenium complex dyes and I^-/I_3^- redox couple. When the dye absorbs a photon, an electron in the dye is excited in $\sim 10^{-11}$ s [26]. The excited electron can transfer through two competitive processes. One is electron injection into conduction band of TiO_2 in $10^{-13} \sim 10^{-10}$ s. [4, 27] The other is decay to ground state of the dye in $\sim 10^{-8}$ s. [4, 27]. The injected electron diffuses in the TiO_2 in $10^{-8} \sim 10^{-4}$ $cm^2 \cdot s^{-1}$, but also two competitive recombination processes exist[28]. One is electron recombination recombined with I_3^- in the electrolyte in $10^{-3} \sim 1$ s. [4, 27] The other is electron recombination recombined with the dye cation in $10^{-6} \sim 10^{-3}$ s. [4, 27] Additionally, reduction kinetics of the dye cation has also two competition process. One is the recombination recombined with injected electron in the TiO_2, and the regeneration regenerated by I^- in the electrolyte in $10^{-6} \sim 10^{-5}$ s.[4, 27] The kinetics are varied with different conditions of the DSSCs.

The absorbed photon by dye is efficiently extracted as current to an external circuit because of the situation described below. The electron injection efficiency is approximately 100% due to the ultrafast electron injection rate compared with the decay to the ground state of the dye. The diffusion length that the injected electron diffuses before the recombination occurs, can be written as:

$$L = \sqrt{D \cdot \tau} \tag{1-1}$$

where L is the diffusion length, D is the electron diffusion coefficient, and τ is the electron lifetime in the TiO_2. The diffusion length of the typical DSSCs is more than 20 μm. Thus, the all injected electrons can be extracted when the thin thickness of the semiconductor electrodes are employed.

1-5. Power conversion efficiency

The power conversion efficiency (PCE) is calculated from

$$PCE(\%) = \frac{V_{OC}\ (\mathrm{V}) \times J_{SC}\ (\mathrm{mA \cdot cm^{-2}}) \times FF}{100\ (\mathrm{mW \cdot cm^{-2}})} \times 100 \tag{1-2}$$

where V_{oc} is the open circuit voltage, J_{sc} is the short circuit current, and FF is the fill factor of the cell. The fill factor is calculated from

$$FF = \frac{V_{max} \times J_{max}}{V_{OC} \times J_{SC}} \quad (1\text{-}3)$$

where V_{max} and J_{max} are the maximum power point voltage and current, respectively. The *FF* is the ratio between the product of V_{max} and J_{max} and the product of V_{OC} and J_{SC}. Therefore, improvements of V_{oc}, J_{sc} and *FF* are necessary to obtain high power conversion efficiency in the dye-sensitized solar cells. Especially, V_{OC} and J_{SC} improvements have large impact on the power conversion efficiency. This is because the *FF* has been obtained relatively high value over 70%[11, 14, 18].

1-5-1. Short circuit current

The short circuit current obtained the required superior values of the current using strategies for each factor that determine the current value. The short circuit current is dependent on the incident photon-to-current-conversion efficiency (IPCE). The IPCE is determined by the product of three yields at each wavelength as follows: the light harvesting efficiency $\boldsymbol{\Phi}_{LHE}$; the electron injection efficiency from dye into the semiconductor $\boldsymbol{\Phi}_{inj}$; and the charge collection efficiency $\boldsymbol{\Phi}_{coll}$ [4]. The IPCE equation is as follows:

$$\text{IPCE} = \boldsymbol{\Phi}_{LHE} \times \boldsymbol{\Phi}_{inj} \times \boldsymbol{\Phi}_{coll} \quad (1\text{-}4)$$

Improvement of the light harvesting efficiency has been obtained by the choice of ligands for

complex dyes[29], the extension of the π-conjugated system of the dyes[17], and the coadsorption of dyes of different absorption wavelength regions[13]. High electron injection efficiency is ensured by the ultrafast electron injection rate compared with the recombination kinetics between the injected electron and the dye cation[27], the suppression of dye aggregation[30], and the control of the free energy difference between the LUMO of the dye and the conduction-band edge of the semiconductor. The charge collection efficiency can reach almost 100% by using a thinner semiconductor electrode than a diffusion length of the electrons in the semiconductor electrode. Meanwhile, the light harvesting efficiency was sufficiently high for thin electrodes. This high light harvesting efficiency is enabled by the use of semiconductor electrodes having a higher roughness factor[7]. Factors influencing electron injection efficiency have been discussed over the years, and strategies for achieving high injection efficiency have been mostly clarified [31, 32].

1-5-2. Open circuit voltage

In contrast with the short circuit current, the open circuit voltage has not readily obtained the expected high open circuit voltage by replacing the redox couples. The highest reported efficiency of a DSSC is 13.0% for a DSSC using SM315 dye in a cobalt complex redox system[10]; the corresponding solar cell parameters are: *Voc* = 0.91 V, *Jsc* = 18.1 mA·cm^{-2}, and *FF* = 0.78%. The spectral edge of the IPCE is 785 nm. A short circuit current of approximately 20 mA·cm^{-2} can be calculated by integrating the region from 350 nm to 785 nm of the air mass 1.5

spectrum when the IPCE is assumed to be 80%. The ratio of the experimental short circuit current to the calculated short circuit current is about 90%. Therefore, the experimental value of the short circuit current was nearly obtained, as expected. However, from the edge of the IPCE spectrum, the energy gap of the dye between the HOMO and LUMO is approximately 1.6 eV. The required free energy difference between the LUMO of dyes and the conduction band edge for electron injection from the dye into the conduction band of a ZnO was estimated to be 0.2 eV [17]. If the required free energy difference between the HOMO of the dye and the redox potential for regeneration is also 0.2 eV, then the open circuit voltage is expected to be 1.2 V. However, the experimental open circuit voltage was determined to be 0.91 V. This open circuit voltage is only 76% of the expected value. The free energy difference value for the regeneration between the HOMO of dye and E_{redox} of 0.2 eV is expected based on the relevant literature[33-35]. To improve the open circuit voltage of DSSCs, many approaches have been proposed. Examples of such approaches are as follows: developing series-tandem type DSSCs , improving an electron's lifetime in the semiconductor electrode by understanding the principle of the reaction between the injected electron and the redox couple [21, 22, 36], and replacing the redox couple with that of more positive redox potential[12]. In particular, the use of a cobalt complex redox couple significantly improved the PCE via an open circuit voltage improvement [13, 14]. For further improvement of the PCE of DSSCs, single-cell DSSCs with higher open circuit voltage are intrinsically required. Thus, expansion of the energy difference between the Fermi level in the

semiconductor and the redox potential of the redox couple is an essential solution. However, the free energy difference between the HOMO of dye and the redox potential becomes narrower as the energy difference between the Fermi level and the redox potential increases. The rate of dye cation reduction is decreased with a narrower free energy difference. As a result, the dye cation can be reduced by the injected electron, thereby decreasing the Fermi level in the semiconductor. Therefore, studies on the reduction kinetics of the dye cation are required. Moreover, the electron lifetime is changed by replacing the redox couple. However, the electron lifetime is mainly studied for the typical redox couple of I^-/I_3^-. Therefore, studies on the electron lifetime are still necessary.

1-6. Present issues

1-6-1. Reduction kinetics of dye cation

The dye cation is generated by electron injection from the excited-state dye into the conduction band of the semiconductor electrode. The dye cation is reduced by the redox couple (regeneration). Subsequently, the dye can contribute to the electron injection again. The dye cation can be also reduced by recombination with the injected electron. The efficiency of the reduction by the redox couple is given by:

$$\Phi_{reg} = \frac{k_{reg}}{k_{reg} + k_{rec}} \tag{1-5}$$

where k_{reg} is the rate constant for regeneration and k_{rec} is the pseudo rate constant for recombination. The regeneration kinetics can be approximately fitted by a first-order exponential function[37]. On the other hand, the recombination kinetics cannot be fitted by the first-order exponential function. This is because the rate constant of the recombination reaction has wide distribution[37]. The rate constant of the regeneration reaction and the recombination reaction can be estimated by calculating half of the reaction decay time. To obtain high performance DSSCs, the Φ_{reg} should be 100%.

Here, the reduction rate of the dye cation can be written as:

$$\frac{d[\mathrm{dye}^+]}{dt} = -k_1[\mathrm{dye}^+][\mathrm{I}^-] - k_2[\mathrm{dye}^+][\mathrm{e}^-_{\mathrm{CB}}] \tag{1-6}$$

where k_1 and k_2 are the rate constant, $[\mathrm{dye}^+]$ is the concentration of the dye cation, and $[\mathrm{I}^-]$ is the reductant concentration in the electrolyte. The I^- is reductant if the $\mathrm{I}^-/\mathrm{I}_3^-$ redox couple is chosen, and $[\mathrm{e}^-_{\mathrm{CB}}]$ is the electron concentration in the conduction band of the semiconductor electrode. The rate constants can be expressed using Marcus theory:

$$k_i \propto \frac{2\pi}{\hbar}[H_{ab}]^2 \frac{1}{\sqrt{4\pi\lambda_i k_B T}} \exp[-\frac{(-\Delta G_i + \lambda_i)^2}{4\lambda_i k_B T}] \tag{1-7}$$

where $\hbar$ is Planck's constant, H_{AB} is the electronic coupling between the electron donor and acceptor, ΔG_i is the free energy difference, λ_i is the reorganization energy, which is the sum of

the internal (λ_v) and solvent (λ_s) reorganization energies, k_B is the Boltzmann's constant, and T is the temperature.

The V_{oc} is limited for typical DSSCs that use the I^-/I_3^- redox couple. This limitation occurs because the free energy difference between the HOMO of the dye and the redox potential of the I^-/I_3^- redox couple is approximately 0.4 eV. Recently, a higher value of V_{oc} was reported by replacing the redox couple from the typical I^-/I_3^- couple to the cobalt(II/III) complex couple[38]. The higher V_{oc} is achieved by shifting the redox potential to be more positive. However, the measured values of V_{oc} have not reached the expected values of V_{oc} that were calculated by the difference between redox potentials[12]. This lack of achieving the ideal V_{oc} occurs because the electron lifetime is decreased by increasing the recombination of the injected electron with the redox couple and/or the dye cation[12, 39]. The positive redox potential decreases the free energy difference for the regeneration. As a result, the regeneration rate is slowed and the regeneration efficiency is reduced.

The regeneration rates have been measured for the combination of various dyes and redox couples[12,40,41]. The required free energy difference for the sufficient reduction of the dye cation by the redox couple has been estimated. This free energy difference was found to vary for various combinations of organic materials. Therefore, to obtain a high open circuit voltage with a small free energy difference of the regeneration reaction, the factors that affect the regeneration kinetics should be clarified. The regeneration kinetics have been found to be affected by the

reductant concentration[42, 39]. The factor in the rate constant, the electron coupling effect between the dye-cation and the reductant, has been discussed regarding the regeneration kinetics[39]. The regeneration kinetics can be explained by a continuous-time random walk (CTRW model) introduced by Nelson et al.[43]. This CTRW model describes the process by which the dye cation is reduced by a detrapped electron from trapping sites and effectively reproduces the experimental results of the recombination kinetics' dependence on the electron density in the conduction band. Regarding the rate constant, to examine the factors of the rate constants that affect the recombination kinetics, a ruthenium complex dye system was used[44]. In that study, the recombination kinetics was reported to be affected by the distance affecting the electronic coupling between the HOMO of the dye and the semiconductor electrode surface. In addition, a triphenylamine-based dye system was used[39]. In that study, the reorganization energies of the dyes ranged from 0.59 to 0.70 eV, and the distances between the HOMO of the dye and the surface of the semiconductor electrode ranged from 9.9 to 13.8 Å. That report indicated that the electronic coupling effect by difference of the distance of 3.9 Å on the recombination kinetics is stronger than the difference of the reorganization energy of 0.11 eV.

Previous studies for the reduction kinetics of the dye cation were explained above, and the effect of the electronic coupling and concentration of the redox couple in the electrolyte on the regeneration kinetics were reported[39, 42]. The adsorbed dyes on the semiconductor electrode were usually dense adsorbed. Therefore, a contribution of the HOMO enclosed with adjacent

dyes to the regeneration is open for discussion. This is because it is not clear whether the redox couples penetrate into the adsorbed dye layer. Similarly, regarding the electronic coupling, the effects of the HOMO position and shape in the dyes on the regeneration kinetics are not clear, as prior studies have examined small structural differences of dyes. Thus, comparisons between dyes with different HOMO shapes and investigations of the effect of substituents that do not affect the HOMO level of the dyes are still required.

For the recombination, it is assumed that interfacial reactions of the recombination were followed by the inverted region of Marcus theory[45] because the reorganization energies of the dyes were calculated around 1 eV[36, 46], and the free energy differences of the recombination reaction could be estimated at greater than 1 eV. However, the recombination kinetics is mostly dominated by the diffusion process in the semiconductor electrode. Therefore, whether the interfacial reactions on the recombination was not fully clarified. This is because interfacial reaction is faster than the diffusion process limit, and thus the effect of the interfacial reaction can not be observed. The recombination mechanism, which was based on the CTRW model, assumes that the electron transfer occurs from the conduction band of the semiconductor electrode. However, the energy sites located under the conduction-band edge exponentially. Thus, understanding the recombination reaction becomes complicated. The trapped electron could affect the recombination kinetics.

1-6-2. Electron lifetime

The electron lifetime (τ) is one of the important factors that determine the open circuit voltage. The electron lifetime is the recombination time for the injected electron in an semiconductor electrode. The recombination occur through two processes, R1 and R2. The R1 process denotes the recombination with I_3^-, and the R2 denotes recombination with the dye cation. The relationship between the electron lifetime and the electron density in the semiconductor electrode is written by the equation:

$$\frac{dn}{dt} = G - \frac{n}{\tau} \tag{1-8}$$

where *n* is the electron density in the semiconductor electrode, *t* is the time, and *G* is the electron generation rate[47]. In the steady state, the electron density is given by

$$n = Gt \tag{1-9}$$

This equation indicates that a longer electron lifetime results in a greater electron density. The Fermi level of the semiconductor electrode is given by

$$E_F = E_{CB} + k_B T \ln \frac{n_{CB}}{N_{CB}} \tag{1-10}$$

where E_F is the Fermi level, E_{CB} is the conduction-band edge energy of the semiconductor

electrode, k_B is the Boltzmann's constant, T is temperature, n_{CB} is the electron density in the conduction band, and N_{CB} is the effective density of states of the conduction-band[48]. This equation indicates that the Fermi level increases with increasing electron density. Thus, a high open circuit voltage is obtained by increasing the electron lifetime.

To obtain a longer electron lifetime, the effects of the electron lifetime on the open circuit voltage and the factors that affect the electron lifetime have been studied. For the R2 regarding the recombination between the injected electron and the dye cation, they are described on section 1-6-1. To improve the electron lifetime, investigations of the interfaces, which are electrolyte/FTO and electrolyte/semiconductor/dye, have been performed. Cameron et al. examined a dense TiO_2 layer on FTO glass. The dense layer decelerated the recombination between the electrons in the FTO and the I_3^- in the electrolyte[49]. Palomares et al. introduced insulating layers to the semiconductor electrode surface[50]. The insulating layers increased the electron lifetime. The TiO_x layer derived from $TiCl_4$ treatment also increased the electron lifetime[51]. Nakade et al. investigated the effect of ionic radii differences on the electron lifetime and the conduction-band edge[36]. Concerning the relationship between the electron lifetime and the structure of dyes, Miyashita et al. demonstrated that the alkyl chains on the dyes in DSSCs extend the distance between the I_3^- and the TiO_2 surfaces[21], which enabled the electron lifetime to be increased. Mosconi et al. reported a quantum chemical calculation result that the short electron lifetime of DSSCs using a ruthenium complex dye with an electrolyte containing a

cobalt complex redox couple system was caused by the attraction of the redox species by the dye[52]. As described above, the blocking effect that is the extension of the distance between the semiconductor surface and the electron acceptor in the electrolyte, and the electron acceptor concentration around the semiconductor surface, contributes to electron lifetime improvement mostly without a trade-off relationship between the electron lifetime and the conduction-band potential. The dispersion force derived from the dye's induced dipole moment also attracts redox species[48], thereby reducing the electron lifetime. The effect of the dispersion force could be smaller than the blocking effect of the dyes on the electron lifetime because the electron lifetimes are increased with increasing the adsorbed dyes amount[21]. Thus, it is unclear whether the dispersion force affects the electron lifetime. The effect of the dispersion force on the electron lifetime is open to discuss.

To improve the electron lifetime, a hypothesis of factors that affect the lifetime as well as a detailed investigation into the hypothesis are needed. For the detailed investigation into the electron lifetime, a proper understanding of the measurement method for the electron lifetime and the development of a novel measurement method for the electron lifetime according to specific aims are required. Several methods have been developed to measure the electron lifetime. These include the following examples.

(1) The pulsed method. The electron lifetime is obtained from the voltage transient that is induced by the absorption of light from a pulsed laser [53]. This method produces results that

are simple to analyze to determine the electron lifetime, but the equipment is relatively expensive.

(2) The impedance spectroscopy method[54] and light intensity modulated method[55]. These methods can provide significant information regarding the surface electron transfer characteristics simultaneously, but the analyses are complex.

(3) The stepped methods[56,57]. The electron lifetime is obtained from the voltage transient that is induced by the absorption of stepped light. One of the stepped methods is the stepped light-induced transient measurements of the photocurrent and voltage (SLIM-PCV) method. The other is the open-circuit voltage-decay (OCVD) technique. There methods are simple to implement.

The SLIM-PCV method is one of the more useful techniques because it allows the electron lifetimes to be obtained quickly and with sufficient precision and easy interpretation. The SLIM method requires a uniform electron generation along the thickness of the photo-electrode; that is, the electron density in each semiconductor particle of the photo-electrode should be the same. However, the measurable condition, which is the degree of uniformity of the electron density, has not been demonstrated clearly.

In the above methods, the electron lifetime is measured by measuring the quasi Fermi level response induced by photoirradiation. For systematic experiments, the development of a novel electron lifetime-measurement method is desired to distinguish the photoirradiation effect

from the electron lifetime under the operating condition. An external power supply circuit can be used for the electron injection from the FTO side to measure the electron lifetime without using electron injection from the dyes. During the impedance measurement, the Fermi levels can be controlled by electron injection into semiconductor electrode from the external circuit[58]. Thus, the electron lifetime is measured even without the electron injection from the dyes. In contrast, a SLIM-PCV method using the external circuit system for electron injection has not been developed.

1-7. Goals of this thesis

In this thesis, the following goals were set.

- Propose a design guide of the molecular structure: To achieve this aim, the effects of the molecular structure difference on the reduction kinetics of the dye cation were investigated.
- Measure the accurate electron lifetime using the SLIM-PCV method: To achieve this, the effects of uniformity of the electron density in the semiconductor electrode on the appeared electron transfer kinetics in DSSCs were investigated.
- Develop a novel method to measure the electron lifetime. A novel method using the external circuit for the electron injection into the semiconductor electrode was developed.
- Obtain a longer electron lifetime. To do this, the relationship between the molecular structure of the dyes and the attraction effects of the dye molecule to the redox couple

surrounding the dye were determined.

1-8. Brief descriptions of chapters

In Chapter 1, the purpose of this thesis concerning electron transfers in DSSCs is described, following a short history of DSSCs and their status in the research.

Chapter 2 outlines the fabrication procedures and explains the characterization methods of DSSCs. The analysis of the experimental data also explains how the transient absorption decays indicate the reduction kinetics of the dye cation.

In Chapters 3 and 4, the structure effect of donor-π-conjugated linker-acceptor (D-π-A) type organic dyes on the reduction kinetics of the dye cation is investigated. The dye cation is reduced by the reductant of a redox couple in the electrolyte (regeneration) or by an injected electron into the semiconductor electrode (recombination). Marcus theory is employed to explain the differences between the reduction kinetics of the dye cation and various structure dyes. In Chapter 3, the effects of the different donor structures on the reduction kinetics are examined. One result demonstrates an effect on regeneration kinetics based on the position of the HOMO in the dye. The HOMO position affects the electronic coupling between the dye cation and I^- in the electrolyte. Another result shows that the recombination kinetics is not followed by a variance in the free energy between the HOMO level of the dye and the conduction-band edge potential. In Chapter 4, the effects of the alkyl chains on the dyes are examined, revealing that the

introduction of the alkyl chain to the π-conjugated linker of the dye decelerates both the regeneration and recombination rates.

In Chapters 5 and 6, the electron lifetime in the semiconductor electrode is investigated. In Chapter 5, to measure the electron lifetime using the SLIM-PCV method, the effects of the required uniformity of the electron density in the semiconductor electrode on the electron transfer kinetics in DSSCs are investigated. To measure the electron lifetime without the injection from dyes, a novel method was developed. This method introduces the external circuit for the electron injection into the semiconductor electrode. In Chapter 6, the relation between the electron lifetime and the effect of attraction by dye molecule is investigated, and a long electron lifetime was obtained by suppressing the dispersion force.

Chapter 7 is the conclusion of the thesis. From the experimental results, I express my views concerning the improvement of the PCE of DSSCs.

1-9. Reference

1 D. S. Ginley, and D. Cahen, Fundamentals of Materials for Energy, 2012. Cambridge university press. Part 1.

2 New Energy and Industrial Technology Development Organization. “NEDO 再生可能エネルギー技術白書 第 2 版”, 2014, Morikita Publishing, ISBN978-4-627-62502-0, Printed in Japan. Chapter 1.

3 M. Xu, S. Wenger, H. Bala, D. Shi, R. Li, Y. Zhou, S. M. Zakeeruddin, M. Grätzel, and P.

Wang, *J. Phys. Chem. C*, 2009, **113**, 2966–2973.

4 A. Hagfeldt, G. Boschloo, L. Sun, L. Kloo, and H. Pettersson, *Chem. Rev.*, 2010, **110**, 6595–9993.

5 F. C. Krebs, S. A. Gevorgyan, and J. Alstrup, *J. Mater. Chem.*, 2009, **19**, 5442–5451.

6 H. Tsubomura, M. Matsumura, Y. Nomura, and T. Amamiya, *Nature*, 1976, **261**, 402–403.

7 B. O'Regan and M. Grätzel, Nature, 1991, **353**, 737–740.

8 M. K. Naxeeruddin, A. Kay, I. Rodicio, R. Humphry-Baker, E. Müller, P. Liska, N. Vlachopoulos, and M. Grätzel, *J. Am. Chem. Soc.*, 1993, **115**, 6382–6390.

9 M. K. Nazeeruddin, F. D. Angelis, S. Fantacci, A. Selloni, G. Viscardi, P. Liska, S. Ito, B. Takeru, and M. Grätzel, *J. Am. Chem. Soc.*, 2005, **127**, 16835–16847.

10 Y. Chiba, A. Islam, Y. Watanabe, R. Komiya, N. Koide, and L. Han, Jpn. *J. Appl. Phys.*, 2006, **45**, L638–L640.

11 T. Bessho, S. M. Zakeeruddin, C. -Y. Yeh, E. W. -G. Diau, and M. Grätzel, *Angew. Chem. Int. Ed.*, 2010, **49**, 6646–6649.

12 S. M. Feldt, G. Wang, G. Boschloo, and A. Hagfeldt, *J. Phys. Chem. C*, 2011, **115**, 21500–21507.

13 A. Yella, H.-W. Lee, H. N. Tsao, C. Yi, A. K. Chandiran, M. K. Nazeeruddin, E. W.-G. Diau, C.-Y. Yeh, S. M. Zakeeruddin, and M. Grätzel, *Science*, 2011, **334**, 629–634.

14 S. Mathew, A. Yella, P. Gao, R. Humphry-Baker, B. F. E. Curchod, N. Ashari-Astani, I. Tavernelli, U. Rothlisberger, M. K. Nazeeruddin, and M. Grätzel, *Nature Chemistry*, 2014, **6**, 242–247.

15 D. P. Hagberg, T. Edvinsson, T. Marinado, G. Boschloo, A. Hagfeldt, and L. Sun, *Chem. Commun.*, 2006, 2245–2247.

16 J. Wiberg, T. Marinado, D. P. Hagberg, L. Sun, A. Hagfeldt, and B. Albinsson, *J. Phys.*

Chem. B, 2009, **113**, 3881–3886.

17 K. Hara, T. Sato, R. Katoh, A. Furube, Y. Ohga, A. Shinpo, S. Suga, K. Sayama, H. Sugihara, and H. Arakawa, *J. Phys. Chem. B*, 2003, **107**, 597–606.

18 D. Joly, L. Pelleja, S. Narbey, F. Oswald, J. Chiron, J. N. Clifford, E. Palomares, and R. Demadrille, *Scientific Reports*, 2014, **4**, 1–7.

19 N. Koumura, Z.-S. Wang, S. Mori, M. Miyashita, E. Suzuki, and K. Hara, *J. Am. Chem. Soc.*, 2006, **128**, 14256–14257.

20 D. P. Hagberg, T. Marinado, K. M. Karlsson, K. Nonomura, P. Qin, G. Boschloo, T. Brinck, A. Hagfeldt, and L. Sun, *J. Org. Chem.*, 2007, **72**, 9550–9556.

21 M. Miyashita, K. Sunahara, T. Nishikawa, Y. Uemura, N. Koumura, K. Hara, A. Mori, T. Abe, E. Suzuki, and S. Mori, *J. Am. Chem. Soc.*, 2008, **130**, 17874–17881.

22 T. N. Murakami, N. Koumura, M. Kimura, and S. Mori, *Langmuir*, 2014, **30**, 2274–2279.

23 G. Zhang, H. Bala, Y. Cheng, D. Shi, X. Lv, Q. Yu, and P. Wang, *Chem. Commun.*, 2009, 2198–2200.

24 W. Zeng, Y. Cao, Y. Bai, Y. Wang, and Y. Shi, *Chem. Mater.*, 2010, 1915–1925.

25 T. Uchiyama, T. N. Murakami, N. Yoshii, Y. Uemura, N. Koumura, N. Masaki, M. Kimura, S. Mori, *Chem. Lett.*, 2013, **42**, 453-454.

26 W. Henry, C. G. Coates, C. Brady, K. L. Ronayne, P. Matousek, M. Towrie, S. W. Botchway, A. W. Parker, J. G. Vos, W. R. Browne, and J. J. McGarvey, *J Phys Chem A*, 2008, **112**, 4537–4544.

27 A. Listorti, B. O'Regan, and J. R. Durrant, *Chem. Mater.*, 2011, **23**, 3381–3399.

28 S. Nakade, T. Kanzaki, Y. Wada, S. Yanagida, *Langmuir*, 2001, **21**, 10803-10807.

29 P. Péchy, T. Renouard, S. M. Zakeeruddin, R. Humphry-Baker, P. Comte, P. Liska, L. Cevey, E. Costa, V. Shklover, L. Spiccia, G. B. Deacon, C. A. Bignozzi, and M. Grätzel, *J. Am. Chem.*

Soc., 2011, **123**, 1613.

30 J. J. He, G. Benko, F. Korodi, T. Polivka, R. Lomoth, B. Akermark, L. C. Sun, A. Hagfeldt, and V. Sundstrom, *J. Am. Chem. Soc.,* 2002, **124**, 4922.

31 H. Matsuzaki, T. N. Murakami, N. Masaki, A. Furube, M. Kimura, and S. Mori, *J. Phys. Chem. C*, 2014, **118**, 17205.

32 R. Katoh, A. Furube, A. V. Barzykin, H. Arakawa, and M. Tachiya, *Coord. Chem. Rev.*, 2004, **248**, 1195–1213.

33 S. Wenger, P.-A. Bouit, Q. Chen, J. Teuscher, D. Di Censo, R. Humphry-Baker, J.-E. Moser, J. L. Delgado, N. Martín, S. M. Zakeeruddin, and M. Grätzel, *J. Am. Chem. Soc.*, 2010, **132**, 5164–5169.

34 S. M. Feldt, G. Wang, G. Boschloo, and A. Hagfeldt, *J. Phys. Chem. C*, 2011, **115**, 21500-21507.

35 T. Daeneke, A. J. Mozer, Y. Uemura, S. Makuta, M. Fekete, Y. Tachibana, N. Koumura, U. Bach, and L. Spiccia, *J. Am. Chem. Soc.*, 2012, **134**, 16925-16928.

36 S. Nakade, T. Kanzaki, W. Kubo, T. Kitamura, Y. Wada, and S. Yanagida, *J. Phys. Chem. B*, 2005, **109**, 3480–3487.

37 J. Nelson and R. E. Chandler, *Coord. Chem. Rev.*, 2004, **248**, 1181–1194.

38 S. M. Feldt, E. A. Gibson, E. Gabrielsson, L. Sun, G. Boscloo, and A. Hagfeldt, *J. Am. Chem. Soc.*, 2010, **132**, 16714–16724.

39 S. M. Feldt, P. W. Lohse, F. Kessler, M. K. Nazeeruddin, M. Grätzel, G. Boschloo, and A. Hagfeldt, *Phys. Chem. Chem. Phys.*, 2013, **15**, 7087–7097.

40 S. Wenger, P. -A. Bouit, Q. Chen, J. Teuschir, D. D. Censo, R. Humphry-Baker, J. -E. Moser, J. L. Delgado, N. Martín, S. M. Zakeeruddin, and M. Grätzel, *J. Am. Chem. Soc.*, 2010, **132**, 5164–5169.

41 T. Daeneke, A. J. Mozer, Y. Uemura, S. Makuta, M. Fekete, Y. Tachibana, N. Koumura, U. Bach, and L. Spiccia, *J. Am. Chem. Soc.*, 2012, **134**, 16925–16928.

42 I. Montanari, J. Nelson, and J. R. Durrant, *J. Phys. Chem. B*, 2002, **106**, 12203–12210.

43 J. Nelson and R. E. Chandler, *Coord. Chem. Rev.*, 2004, **248**, 1181-1194.

44 J. N. Clifford, E. Palomares, M. K. Nazeeruddin, M. Grätzel, J. Nelson, X. Li, N. J. Long, and J. R. Durrant, *J. Am. Chem. Soc.*, 2004, **126**, 5225–5233.

45 R. A. Marcus and N. Sutin, *Coord. Chem. Rev.*, 1985, **811**, 265-322.

46 D. Moia, V. Vaissier, I. López-Duarte, T. Torres, M. K. Nazeeruddin, B. C. O'Regan, J. Nelson, and P. R. F. Barnes, *Chem. Sci.*, 2013, **5**, 281-290.

47 S. Nakade, T. Kanzaki, Y. Wada, and S. Yanagida, *Langmuir*, 2001, **21**, 10803–10807.

48 A. Kunioka, and K. Kamimura, 1996, "Shinban Kisohandoutai Kougaku (Fundamentals of Semiconductor Engineering), Asakura Publishig, ISBN4-254-22138-X, Printed in Japan.

49 P. J. Cameron and M. J. Peter, *Phys. Chem. B*, 2005, **109**, 7392–7398.

50 E. Palomares, J. N. Clifford, S. A. Haque, T. Lutz, and J. R. Durrant, *J. Am. Chem. Soc.*, 2003, **125**, 475–482.

51 B. C. O'Regan, J. R. Durrant, P. M. Sommeling, and N. J. Bakker, *J. Phys. Chem. C*, 2007, **111**, 14001-14010.

52 E. Mosconi, J. -H. Yum, F. Kessler, C. J. G. García, C. Zuccaccia, A. Cinti, M. K. Nazeeruddin, M. Grätzel, and F. D. Angelis, *J. Am. Chem. Soc.*, 2012, **134**, 19438–19453.

53 B. C. O'Regan, K. Bakker, J. Kroeze, H. Smit, P. Sommeling, and J. R. Durrant, *J. Phys. Chem. B*, 2006, **110**, 17155-17160.

54 F. Fabregat-Santiago, G. Garcia-Belmonte, I. Mora-Seró, and J. Bisquert, *Phys. Chem. Chem. Phys.*, 2011, **13**, 9083-9118.

55 J. van de Lagemaat, N. G. Park, and A. J. Frank, *J. Phys. Chem. B*, 2000, **104**, 2044-2052.

56 A. Zaban, M. Greenshtein, and J. Bisquert, *Chem. Phys. Chem.*, 2003, **4**, 859-864.

57 S. Nakade, T. Kanzaki, Y. Wada, and S. Yanagida, *Langmuir*, 2005, **21**, 10803-10807.

58 F. Fabregat-Santiago, J. Bisquert, G. Garcia-Belmonte, G. Boschloo, and A. Hagfeldt, *Sol. Energy Mater. Sol. Cells*, 2005, **87**, 117-131.

Chapter 2

Experimental

Chapter 2. Experimental

DSSCs are easily fabricated; however, the electron transfer mechanism is complex and derived from many kinds of electron transfer processes. The time scale of the electron transfer rate at each interface varies widely from picosecond to millisecond orders. In this chapter, the fabrication method and the characterization methods of the DSSCs are described.

2-1. Fabrication of the DSSCs

Figure 2-1 shows a schematic cross section of the DSSCs. This type of cells were employed for the I-V characterization, the IPCE spectrum measurement and the transient absorption measurement except the transient absorption measurement using 3 electrode reference electrode system. The DSSC comprises a photo-electrode, electrolyte containing redox couple, and platinum sputtered FTO glass as the counter electrode. In this thesis, the photo-electrodes were prepared by depositing a paste that included TiO_2 nano-particles (18NR, CCIC or PST-18NR, Dyesol) on FTO glass (SnO2:F, AGC Fabritech). The selected redox couple was the I^-/I_3^-. The photo-electrodes were attached to platinum counter electrodes by thermal adhesive film. The pores of the photo-electrodes were filled by the electrolyte through two holes in the counter electrode. The holes were sealed with the thermal adhesive film and a glass. Figure 2-2 shows a schematic procedure for the fabrication of the DSSCs.

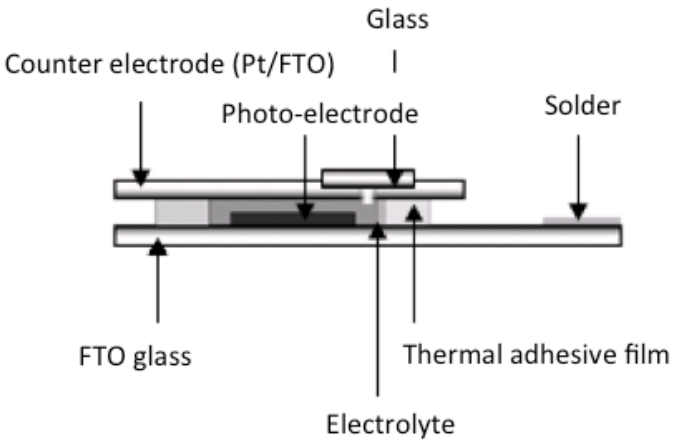

Figure 2-1. Schematic cross section of the DSSCs. Pores of the photo-electrode are filled by the electrolyte; electrolyte is sandwiched between the photo-electrode and counter electrode; solder collects electrons.

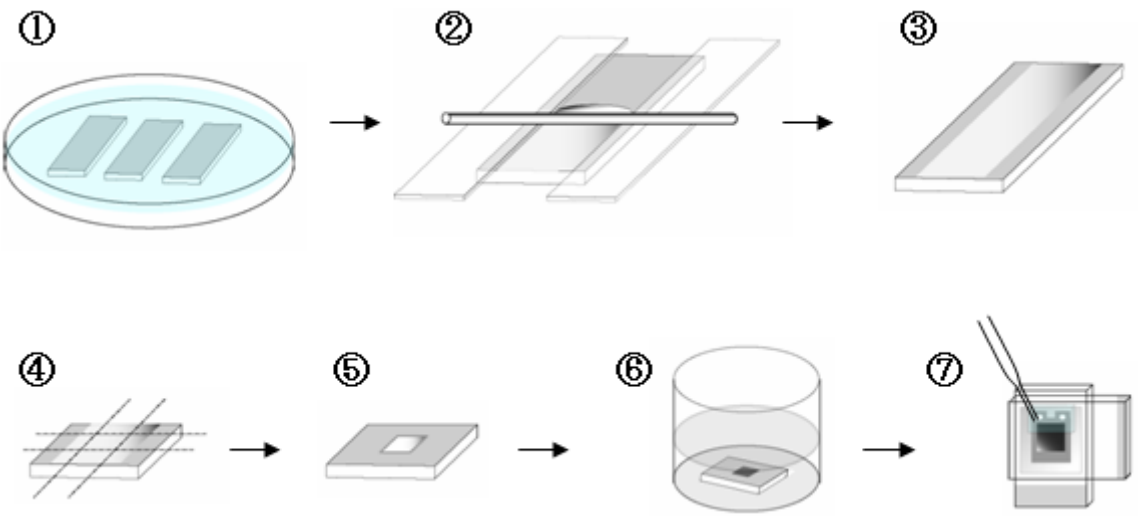

Figure 2-2. Schematic procedure for fabrication of the DSSCs. (1) Washing FTO glasses, (2) deposition of paste, (3) sintering semiconductor electrodes, (4) cutting and shaving semiconductor electrode, (5) reheating semiconductor electrode before immersing, (6) dye adsorption onto semiconductor surface, (7) assembling DSSCs.

Each step in Figure 2-2 is outlined below.

(1): Washing the FTO glass

The FTO glasses were washed by ultrasonication with 2-propanol for 10 min, neutral detergent containing distilled water for 10 min, and plain distilled water for 10 min. After ultrasonication, the FTO glasses were washed with UV ozone for 25 min.

(2): Deposition of TiO_2 paste

Mending tapes were placed on the side edges of the FTO substrates. The TiO_2 paste was deposited on the FTO substrate by squeegee method.

(3): Sintering the semiconductor electrodes

The porous TiO_2 electrodes were obtained by sintering the deposited substrate for 30 min with 30 min ramp time by electric furnace.

(4): Cutting and shaving the semiconductor electrode

The sintered TiO_2 electrodes were cut to 1.2 × 2 cm. The deposited TiO_2 face was shaved to 5 × 5 mm by a slide glass.

(5): Reheating the semiconductor electrode

The semiconductor electrodes were reheated to 450°C by the electric furnace or a hotplate, to remove adsorbed organic materials and water as a pretreatment for immersing.

(6): Dye adsorption onto the semiconductor surface

The photo-electrodes that the dye adsorbed on the surface of the semiconductor

electrode were obtained by immersing the semiconductor electrode into a dye solution at 90°C and maintaining it for 12 ~ 18 hours at 25°C in the dye solution. The amount of the adsorbed dyes was strongly affected by the temperatures.

(7): Assembling the DSSCs

After the adsorption, the photo-electrodes were rinsed with solvents of the dye solutions. The thermal adhesive film was employed as a spacer between the counter and the photo-electrode. The electrolyte was injected into the space between the counter and the photo-electrode through the holes in the counter electrode. The holes were sealed by thermal adhesive film and the slide glass.

2-2. I-V characteristic

Figure 2-3 shows the typical I-V curve of the DSSCs.

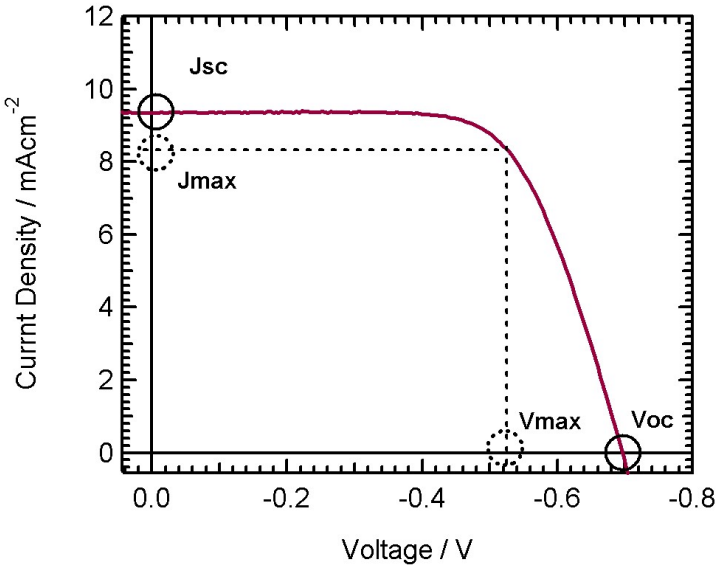

Figure 2-3. Typical I-V curve of the DSSCs. I-V curves were obtained by plots of currents at each applied voltage; Sourcemeter was used to apply the voltage; N719 dye was employed; electrolyte was 0.1 M LiI, 0.6 M DMPImI, 0.05M I_2, and 0.6 M *t*BP in acetonitrile.

The I-V measurements were performed under a solar simulator (YSS-100A, Yamashita Denso). The solar simulator was tuned to air mass (AM) 1.5 spectrum by an AM 1.5 filter[1]. The I-V curves were obtained by plots of currents at each applied voltage. A sourcemeter (2400, Keithley Instruments) was used to apply the voltage and to collect the current. The J_{max} was the current at the maximum power obtained load. The V_{max} was the voltage at the maximum power obtained load.

2-3. IPCE spectrum measurement

For current characterization, the IPCE spectrum measurements are important. The IPCE is quantum efficiency as written below:

$$IPCE\ (\%) = \frac{Number\ of\ collected\ electron}{Number\ of\ incident\ photon} \times 100 \qquad (2\text{-}1)$$

The number of incident photons was counted by a Si photodiode (Hamamatsu S1337-1010BQ) at each wavelength. The number of collected electrons was calculated from the short circuit current at each wavelength. During the current measurement, a mask was employed on the active area of the DSSCs to avoid the reflection of the source light by the glass edge. The masked area was 3 × 3 or 4 × 4 mm.

2-4. Transient absorption measurement

The transient absorption measurement was employed for the reduction kinetics evaluation of the dye cation.

2-4-1. Principle of transient absorption measurement

The transient absorption measurement can be used to measure the transient species spectrum and kinetics. The transient species were generated by pulsed pump laser. The spectrum was calculated by an optical density (OD) measurement at each wavelength of the probe light.

The kinetics was measured by recording the decay absorbed by the transient species of the OD at a wavelength. The OD is written below.

$$OD = -\log(T) \tag{2-2}$$

$$T_i = I_i / I_0 \tag{2-3}$$

$$T_f = I_f / I_0 \tag{2-4}$$

$$\Delta OD = OD_f - OD_i = -\log(T_f) + \log(T_i) = \log\left(\frac{T_i}{T_f}\right) = \log\left(\frac{I_i}{I_f}\right) \tag{2-5}$$

where T is the transmittance, I is the intensity of the probe light, T_i is the transmittance of probe light without the transient species, T_f is the transmittance of probe light with the transient species, I_0 is the initial intensity of the probe, I_i is the transmitted light intensity without the transient species, and I_f is the transmitted light intensity with the transient species. The ΔOD indicates an absorbance of transient species.

2-4-2. Transient absorption measurement of dye cation

The dye cation absorbs near-infrared region wavelength light[2]. The transient absorptions of the dye cations can be measured by measuring a transient of transmitted light of the near-infrared region wavelength light that is used as a probe light[2, 3]. The pump laser to generate dye cation should be chosen at a wavelength absorbed by the ground state dye.

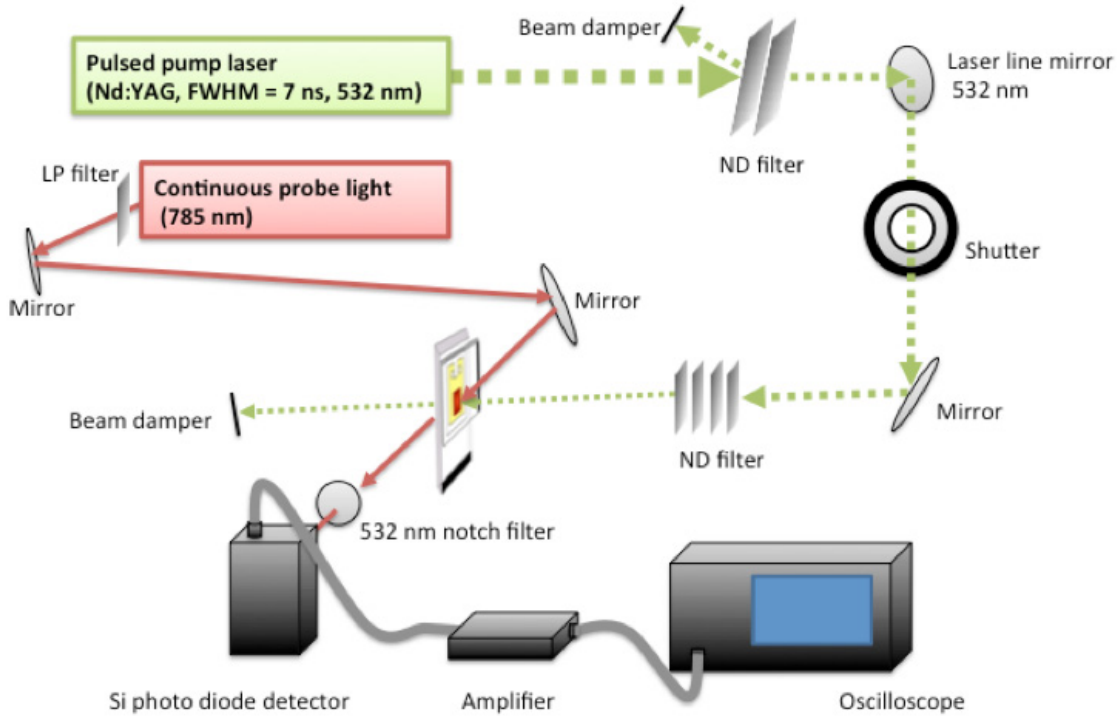

Figure 2-4. Schematic representation of the transient absorption measurement of the dye cation. Nd:YAG was used as pulsed pump laser; continuous light was used as probe light; dye cation decay signal was detected by Si photodiode; detected signal was amplified by amplifier; amplified signal was collected by oscilloscope.

Figure 2-4 shows a schematic representation of the transient absorption measurement system of the dye cation. Here, an Nd:YAG pulsed pump laser (Spectra Physics, Quanta-Ray, FWHM = 7 nm, 532 nm) was used as pump laser. A continuous laser probe light (Coherent, Lab-laser, 785 nm) was employed as probe light for the reduction kinetics measurement. The transmittance signal of the probe light was detected by a Si photodiode (Model 1621, New Focus). The transmittance signal difference was quite small (ΔOD was usually less than 10^{-3}

order). Therefore, the detected signal was intensified by an amplifier (Voltage Amplifier DHPVA, FEMTO, DC mode, 10–40dB). The amplified signal was collected by an oscilloscope (Tektronix). To average the transient, 4–256 shots of decay were collected.

2-4-3. Transient absorption kinetics of dye cation

The dye cation reduction kinetics includes two electron transfer routes. One is the reduction reduced by the redox couple (regeneration), and the other is the reduction reduced by the electron injected into the semiconductor electrode (recombination). To obtain high performance DSSCs, a regeneration efficiency that is the ratio of the regeneration to the recombination should be 100%. The recombination causes lower open circuit voltage and short circuit current. The regeneration efficiency can be written as[4]:

$$\Phi_{reg} = \frac{k_{reg}}{k_{reg} + k_{rec}} \approx 1 - \frac{t_{1/2,redox}}{t_{1/2,inert}} \qquad (2\text{-}6)$$

where k_{reg} is the rete constant for the regeneration, k_{rec} is the rate constant for the recombination, $t_{1/2,redox}$ is the half time of the decay on the transient absorption kinetics measurement of photo-electrodes using redox couple congaing electrolytes and $t_{1/2,redox}$ is the half time of that of photo-electrodes using without redox couple electrolytes. The rete constants can be expressed inverse of the half time of the decays[4, 5].

Comparison of the reduction rate of the dye cation was used half time of the transient

absorption decay. Figure 2-5 shows examples of the transient absorption kinetics of dye cations. ΔOD signals are decreasing with time, and half times of the kinetics are indicated. The half time of the measured cell using redox couple containing electrolyte is shorter than that of the measured cell using without redox couple electrolyte. This result indicate that the reduction rate of the cell using redox couple containing electrolyte is faster than that of the cell using without redox couple electrolyte.

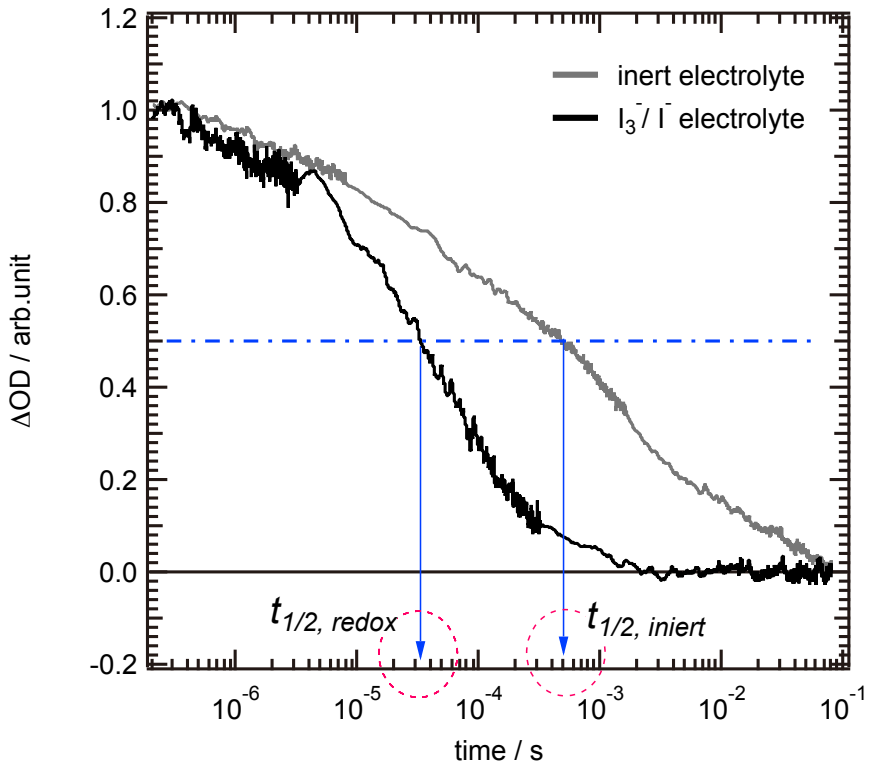

Figure 2-5. Transient absorption kinetics with inert electrolyte and redox electrolyte. Arrows indicate half time of the kinetics. Electrolytes were 0.3 M LiI, 0.05 M I_2 and 0.6 M *t*BP in acetonitrile (I_3^-/I^- electrolyte) and 0.3 M $LiClO_4$ and 0.6 M *t*BP in acetonitrile (inert electrolyte).

i) Regeneration kinetics of the dye cation

To measure the regeneration kinetics, the electrolytes containing the redox couple (redox electrolytes) were employed. In this thesis, I^-/I_3^- redox couple was selected. The dye cation was reduced by the not only I^- but also the injected electron. Therefore, the measurements of the dye cation for the regeneration kinetics measurement required confirmation that the reduction kinetics was not affected by the recombination kinetics.

To examine the dye cations dominantly reduced by the I^-, the I-V measurements were performed under the solar simulator with different intensities of solar simulator irradiation, it was examined whether the short circuit current was proportional to the light intensity. When the dye cation was not sufficiently reduced by the redox couple, the short circuit current was not proportional to the light intensity. This is because the recombination between the injected electron and the dye cation was included.

After the I-V examination, the transient absorption kinetics was measured. To examine whether the reduction kinetics was affected by the electron density in the semiconductor electrode, the reduction kinetics was collected with several different intensities of the pump laser. Transient currents were also collected to calculate the electron density in the semiconductor electrode. If the reduction kinetics was not affected by the difference of the electron density, it could be deemed that the dye cation was immediately reduced by the I^-. This consideration is

because the recombination kinetics is accelerated by increasing the electron density in the semiconductor electrode[3].

ii) Recombination kinetics of dye cation with the injected electron

To measure the recombination kinetics, the electrolytes without the redox couple (inert electrolytes) were employed. In the inert electrolyte, the dye cation was reduced by only the injected electron. The recombination kinetics is changed by the electron density difference. The CTRW model explains this electron density dependence[6]. From Marcus theory, it can also be observed that the recombination kinetics is affected by the conduction-band edge potential of the semiconductor electrode. For the analysis, the electron density and the conduction-band edge potential were estimated using a three-electrode electrochemical cell. The effects of various dyes' molecular structures on the recombination kinetics can be measured by comparison at the same electron density.

2-4-4. Transient absorption spectrum of dye cation

The spectra of the dye cations of newly synthesized dyes are unknown. Thus, measurement of the dye cation spectra was required. The dyes were adsorbed on the TiO_2 electrodes. To generate the dye cation, the photo-electrode was irradiated by Nd:YAG laser. The Xe lamp (AT-100HG, Shimadzu) with a monochromator (PSG-120S, Shimadzu, slit width = 4

mm) was used for the probe light. The *Δ*OD was measured at each wavelength. Figure 2-6 shows an example of the transient absorption spectrum measurement results. The electron densities were measured simultaneously with the transient absorption measurements. The electron density relates to a measure of the generated dye cation. The OD increased proportionally with the electron density. The minus OD means a bleaching. The bleaching occurred with decreasing ground state absorption of the dye. To only measure the reduction kinetics of the dye cation, the wavelength of the probe light should be avoided the wavelength that exist both absorption of the ground state dye and the dye cation.

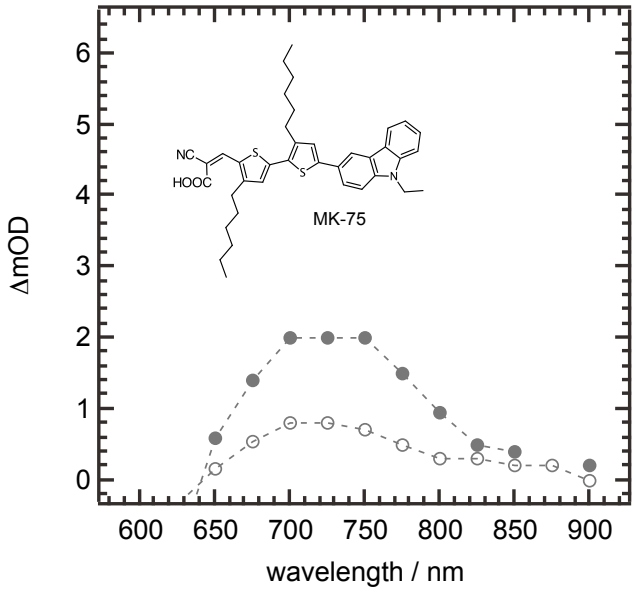

Figure 2-6. Dye cation absorbance spectra. Dye was organic MK-75; electrolyte composition was 0.1 M LiI, 0.6 M DMPImI, 0.05 M I_2, and 0.5 M *t*BP in acetonitrile; electron density of the closed symbol was 4.8×10^{17} cm^{-3} and of the open symbol was 1.6×10^{17} cm^{-3}.

2-5. References

1 JIS C 8912:2011, Japanese Industrial Standards, Solar simulators for crystalline solar cells and modules.

2 R. Katoh, A. Furube, S. Mori, M. Miyashita, K. Sunahara, N. Koumura, and K. Hara, *Energy Environ. Sci.*, 2009, **2**, 542–546.

3 I. Montanari, J. Nelson, and J. R. Durrant, *J. Phys. Chem. B*, 2002, **103**, 12203–12210.

4 S. M. Feldt, P. W. Lohse, F. Kessler, M. K. Nazeeruddin, M. Grätzel, G. Boschloo, A. Hagfeldt, *Phys. Chem. Chem. Phys.*, 2013, **15**, 7087-7097.

5 A. Hagfeldt, G. Boschloo, L. Sun, and L. Kloo, *Chem. Rev.*, 2010, **110**, 6595–6663.

6 J. Nelson and R. E. Chandler, *Coord. Chem. Rev.*, 2004, **248**, 1181–1194.

Chapter 3

Effects of the structure of the donor moiety on dye cation reduction kinetics

Chapter 3. Effects of the structure of the donor moiety on dye cation reduction kinetics

3-1. Introduction

Open circuit voltage of DSSCs is determined by the difference between the Fermi level of TiO_2 and the redox potential of redox couples in electrolyte solutions. Recently, an I^-/I_3^- redox couple was replaced with a cobalt (II/III) complex redox couple. The V_{oc} subsequently increased over 1 V due to the high redox potential of the cobalt(II/III) complex redox couple compared with that of the I^-/I_3^- redox couple[1]. However, a higher V_{oc} is not obtained for many dyes when the redox couple is replaced with the cobalt complexes[2–4]. One possible reason is fast charge recombination between the injected electrons and the dye cations. This recombination can be even accelerated by dye cation's slow regeneration kinetics caused by the small energy difference between the levels of the HOMO of dye and the cobalt complexes (ΔG). When the redox potential is shifted positively, ΔG becomes smaller.

The required energy difference for sufficient regeneration has been estimated by transient absorption studies combined with various dyes and redox couples. The required energy difference values were varied widely 150–400 meV[5,–7] due to the many factors involved in electron transfer kinetics. Therefore, the effective factors should be identified. The electron transfer kinetics is well-explained by Marcus theory[8]. The regeneration and recombination

kinetics have also been investigated with Marcus theory, and the results were also well explained[9,10].

The other factors on the reduction kinetics of dye cation other than the *ΔG* have been also studied. Montanari et al. demonstrated that the regeneration rate were accelerated by high I^- concentration in the electrolyte[11], and also Feldt et al. reported that the regeneration kinetics was accelerated by high concentration of the cobalt complex as reductant in the electrolyte[12]. Effect of the electronic coupling on the regeneration kinetics was also investigated, and the effect on the reduction kinetics was greater than the reorganization energy[13]. On the recombination kinetics, the dependence of distance between semiconductor surface and the donor of dyes has been investigated. When the distance was increased, the recombination kinetics was decreased[13,14]. These experiments were usually performed with DSSCs using dyes having the same donor moiety. The HOMO of the dyes is mostly localized on the donor moiety. The HOMO is assumed to be electron acceptor orbital when the dye is oxidized. Then, it can be considered that the donor moiety electronic structure difference will affect the reduction kinetics of dye cations. Therefore, in this chapter, the effect of donor moiety structure differences on the reduction kinetics is examined to obtain the design guide for the high regeneration efficiency in DSSCs.

The reduction kinetics of the dye cation can be written as:

$$\frac{d[\mathrm{dye}^+]}{dt} = -k_1[\mathrm{dye}^+][\mathrm{I}^-] - k_2[\mathrm{dye}^+][\mathrm{e}^-_{\mathrm{CB}}] \qquad (3\text{-}1)$$

where k_i is the rate constant, [dye$^+$] is the concentration of the dye cation in the DSSCs, [I$^-$] is the concentration of I$^-$ in the electrolytes, [e^-_{CB}] is the electron density in the semiconductor electrode, and t is the time. The rate constant is proportional to an expression below from Marcus theory:

$$k_i \propto \frac{2\pi}{\hbar}[H_{ab}]^2 \frac{1}{\sqrt{4\pi\lambda_i k_B T}} \exp[-\frac{(-\Delta G_i + \lambda_i)^2}{4\lambda_i k_B T}] \qquad (3\text{-}2)$$

where $\hbar$ is Planck's constant, H_{ab} is the electronic coupling between the electron donor and acceptor, ΔG_i is the free-energy difference, λ_i is the reorganization energy, which is the sum of the internal (λ_v) and solvent (λ_s) reorganization energies, k_B is the Boltzmann's constant, and T is the temperature.

3-2. Experimental

DSSCs were fabricated by the procedure described in chapter 2. Donor-π-conjugated linker-acceptor (D-π-A) type metal-free organic dyes examined here employ, carbazole (MK-2), triphenylamine (MK-88), and coumarin (MK-31) as donor. The structures of the dyes are shown in Figure 3-1, and their synthesis procedures are described in the literature[15]. The HOMO levels of the dyes were measured by differential pulse voltammetry. The values of MK-1, MK-88 and MK-31 were 1.1, 1.0 and 0.85 V vs. NHE, respectively. The dyes were dissolved in mixed solvents (AN/Toluene/*t*-BuOH = 1:1:1 for MK-1 and MK-88, AN/t-BuOH/EtOH = 2:2:1 for

MK-31). The concentrations of the dye solutions were approximately 0.2 mM. Photoelectrodes were prepared using the procedures described in chapter 2. The electrolytes were 0.3M LiI, 0.05 M I_2 and 0.6 M *t*BP in acetonitrile (Li electrolyte); 0.3M TBAI, 0.05 M I_2 and 0.6 M *t*BP in acetonitrile (TBA electrolyte); 0.3 M $LiClO_4$ and 0.6 M *t*BP in acetonitrile (Li inert electrolyte); and 0.3 M $TBAClO_4$ and 0.6 M *t*BP in acetonitrile (TBA inert electrolyte). I-V measurements were taken under a solar simulator (Yamashita Denso, YSS-100A), and the light source was tuned to Air Mass 1.5 spectrum and 1 sun (100 $mW \cdot cm^{-2}$). The light intensity was reduced using neutral density filters (ND filter). The IPCE spectrum was measured with a monochromator and a digital multimeter. Transient absorption measurements used a Nd:YAG laser (Spectra Physics, Quanta-Ray, FWHM = 7 ns, 532 nm, 10 Hz) as a pump laser. Excitation frequency by the Nd:YAG laser was reduced by a shutter controlled with a function generator. The transient absorption kinetics of the cells using electrolyte-containing redox couple was not strongly affected by the excitation frequency. The excitation frequency was decreased until the all injected electrons were recombined when the transient absorption kinetics with an inert electrolyte was measured. The transient absorption signals were detected by a Si photo-detector (Model 1621, New Focus) with an amplifier (Voltage Amplifier DHPVA, FEMTO, DC mode, 10–40dB), and the signals were averaged by an oscilloscope (Tektronix).

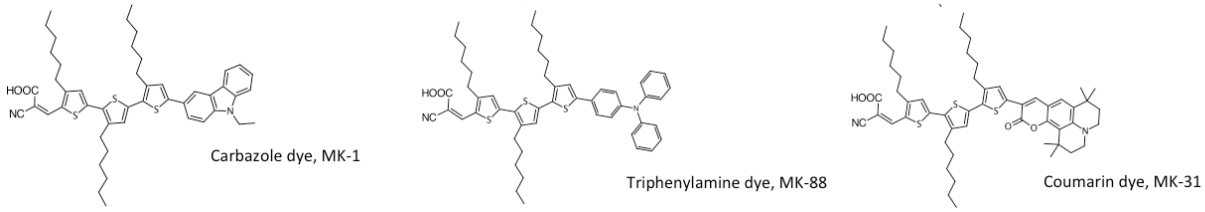

Figure 3-1. Structures of dyes: carbazole dye, MK-1 (HOMO = 1.1 V vs NHE); triphenylamine dye, MK-88 (HOMO = 1.0 V vs NHE); and coumarin dye, MK-31 (HOMO = 0.85 V vs NHE).

3-3. Results and Discussion

The reduction kinetics of the dye cations were evaluated after the measurements of I-V characteristic and IPCE spectra.

3-3-1. I-V characteristics and IPCE spectra

Table 3-1 shows the I-V performance of the DSSCs with the Li electrolyte. The light intensity from the solar simulator was attenuated with ND filters. The values of short circuit current were almost proportional to the light intensity. Thus, a high dye cation regeneration efficiency under this condition was expected. Figure 3-2 shows the IPCE spectra. At a wavelength of 532 nm, the DSSCs efficiently converted photons to electrons. On the other hand, at 785 nm, the DSSCs converted little or no photons to electrons. Therefore, the transient absorption at 785 nm can be used to study the dye cation reduction kinetics.

Table 3-1. I-V characteristics of DSSCs. The DSSCs were measured under three different intensities using a solar simulator. "1 sun" denotes measurement under 100 mW·cm^{-2}, while "ND50" and "ND25" denote an intensity of 1 sun passed through a neutral density filter with a transmittance equal to the specified number. The electrolytes were 0.3 M LiI, 0.05 M I_2 and 0.6 M *t*BP in acetonitrile.

Conditions		V_{oc} / V	I_{sc} / mAcm^{-2}	*FF*	*PCE* /%
MK-1	1 sun	0.69	7.3	0.68	3.4
	ND50	0.67	3.7	0.68	3.4
	ND25	0.64	1.9	0.69	3.4
MK-88	1 sun	0.74	7.0	0.71	3.7
	ND50	0.72	3.6	0.71	3.7
	ND25	0.70	1.9	0.70	3.7
MK-31	1 sun	0.68	8.5	0.67	3.9
	ND50	0.69	4.4	0.69	4.2
	ND25	0.64	2.3	0.69	4.1

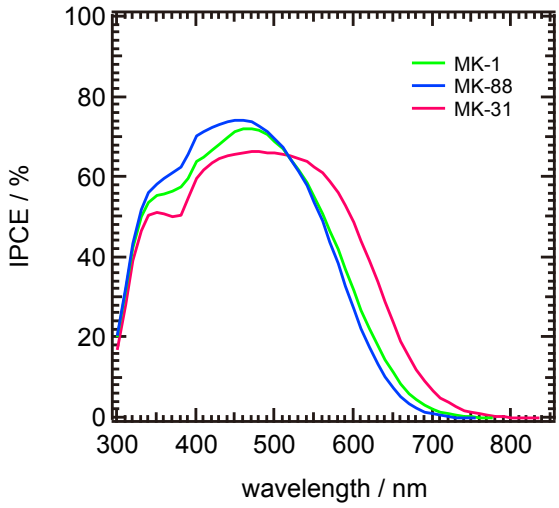

Figure 3-2. IPCE spectra of DSSCs. Electrolytes were 0.3 M LiI, 0.05 M I_2 and 0.6 M *t*BP in acetonitrile. Photons were efficiently converted (approximately 60%) at doubled Nd:YAG laser wavelength, 532 nm. Little or no signals were observed at the laser wavelength of 785 nm. The electrolytes were 0.3 M LiI, 0.05 M I_2 and 0.6 M *t*BP in acetonitrile.

3-3-2. Effect of pump intensity on transient absorption measurements

Transient absorption was measured with various pump laser intensities. Figure 3-3 shows the transient absorption of the dye cation in DSSCs with the Li electrolyte. Table 3-2 shows the Electron densities and decay half time of transient absorption kinetics measurement of DSSCs using MK-1, MK-88 or MK-31 with the Li electrolyte with various pump intensities. Figure 3-4 shows the transient absorption kinetics of the dye cation in the cells with the Li inert electrolyte. The intensity dependences differed between the conditions with and without redox couple. With the electrolyte containing the redox couple, the difference in the kinetics half time between 11 and 200 $\mu J \cdot cm^{-2}$ was 3 times or less. These results suggest that the dye cations were efficiently reduced by I^- in the electrolytes. The little differences of the kinetics half time of DSSCs using these each three dyes were due to high electron density in the TiO_2 at 200 $\mu J \cdot cm^{-2}$. This forecast corresponded to the incompletely linear dependence of the short circuit currents with the light intensity on the I-V measurements (Table 3-1). On the other hand, with the electrolyte without the redox couple, the difference in the kinetics half time between 11 and 200 $\mu J \cdot cm^{-2}$ was 10–20 times. These results suggest that the recombination rate between the injected electrons and the dye cations was accelerated with increasing electron density in the TiO_2 electrodes. These results are consistent with a previous report[16].

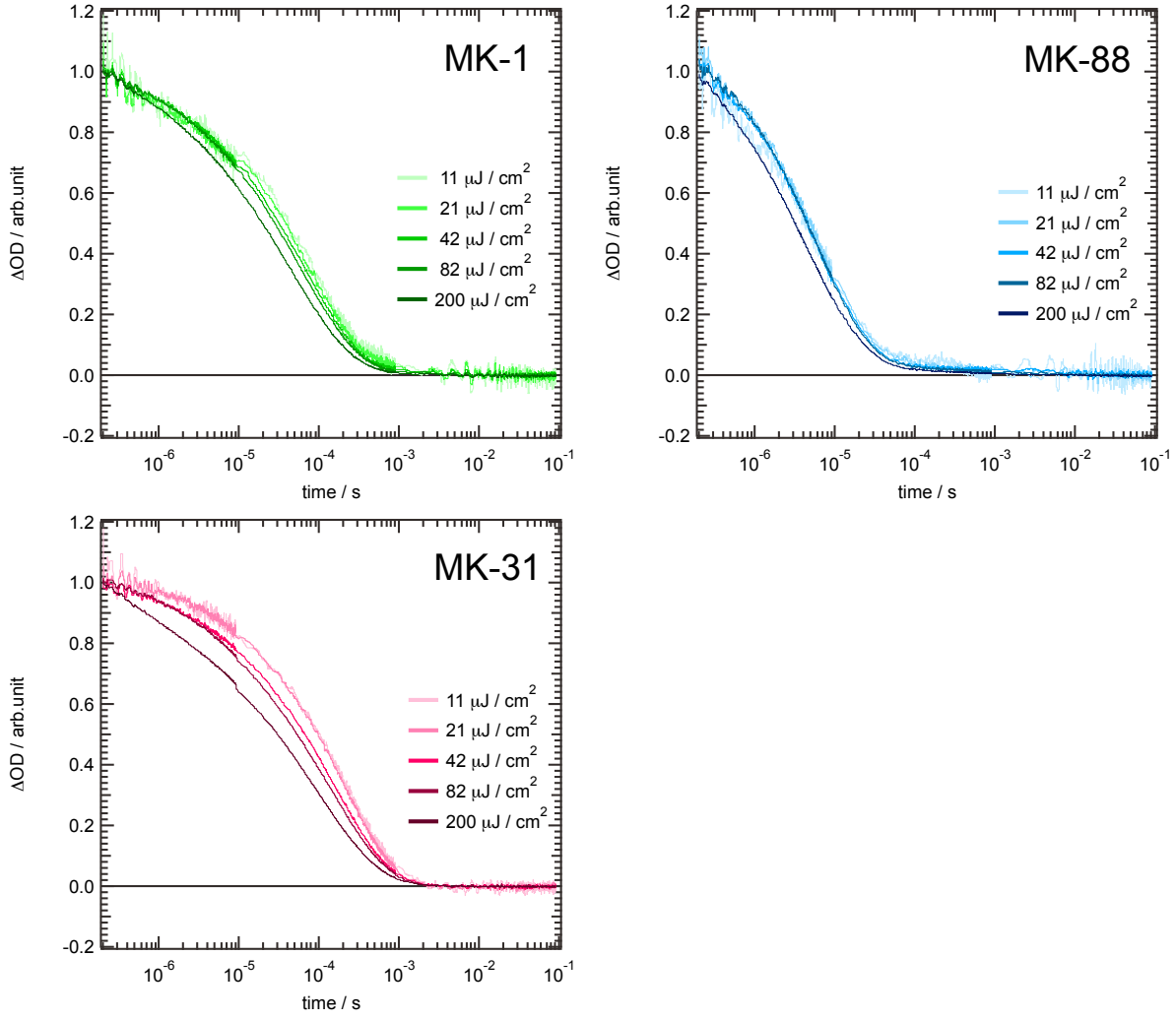

Figure 3-3. Transient absorption of the dye cation of MK-1, MK-88 or MK-31 in DSSCs. Electrolytes were 0.3 M LiI, 0.05 M I_2 and 0.6 M *t*BP in acetonitrile. The dye cation was generated by electron injection from an excited dye induced by a pulsed pump laser. Five levels of pulsed pump laser power were used. The pump laser wavelength was 532 nm, and the probe laser wavelength was 785 nm.

Table 3-2. Electron densities and decay half time of transient absorption measurement of DSSCs using MK-1, MK-88 or MK-31 with various pump intensities. Electrolytes were 0.3 M LiI, 0.05 M I_2 and 0.6 M *t*BP in acetonitrile. Five levels of pulsed pump laser power were used. The pump laser wavelength was 532 nm, and the probe laser wavelength was 785 nm.

Dye	Pump intensity/ $\mu J \cdot cm^{-2}$	electron density/ cm^3	Half time/ μs
MK-1	11	6.5×10^{16}	40
	21	1.4×10^{17}	38
	42	2.8×10^{17}	31
	82	4.8×10^{17}	28
	200	8.7×10^{17}	20
MK-88	11	6.7×10^{16}	4.5
	21	1.5×10^{17}	4.5
	42	2.7×10^{17}	4.5
	82	5.0×10^{17}	4.5
	200	8.9×10^{17}	3.2
MK-31	11	6.5×10^{16}	100
	21	1.4×10^{17}	96
	42	2.8×10^{17}	66
	82	4.8×10^{17}	53
	200	8.7×10^{17}	30

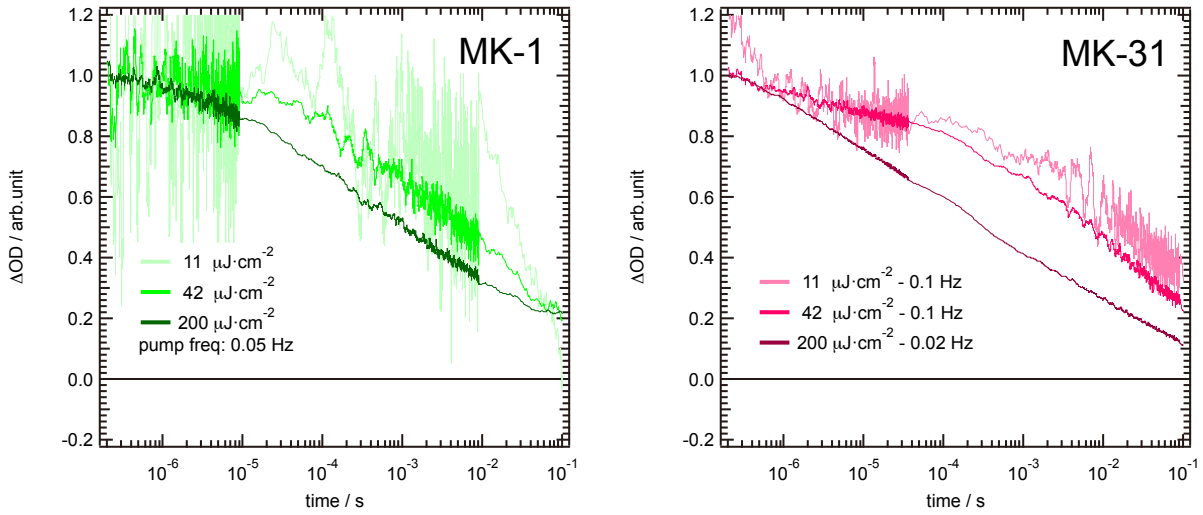

Figure 3-4. Transient absorption kinetics of the dye cation of MK-1 and MK-31. Electrolytes were 0.3 M $LiClO_4$ and 0.6 M *t*BP in acetonitrile. The dye cation was generated by electron injection from an excited dye induced by a pulsed pump laser. Three levels of pulsed pump laser power were used. The powers were 11, 42, and 200 μJ·cm^{-2}. The probe laser wavelength was 785 nm, the pump laser wavelength was 532 nm. The pulse frequency for MK-1 was 0.05 Hz, and that for MK-31 was 0.1 or 0.02 Hz.

3-3-3. Regeneration kinetics of the dye cation

The reduction kinetics of the dye cation was compared among the three dyes in the DSSCs using the Li electrolyte. The results are shown in Figure 3-5 (a). For the measurements, the intensity was set to 42 μJ·cm^{-2}. The half times of the regeneration of MK-1, MK-88 and MK31 were 31 μs, 4.5 μs, and 66 μs, respectively. The *ΔG* between the HOMO of the dye and the I^-/I_3^- redox potential were 0.66, 0.62, and 0.45 eV for MK-1, MK-88 and MK-31, respectively. The *ΔG* was calculated from the I^-/I_3^- redox potential of the redox couple, 0.4 eV. This result shows that the regeneration kinetics were not only controlled by *ΔG*. To explain the results, the I^- concentration around the dye and the electronic coupling were considered. It

appears that the reorganization energy did not change because the molecular sizes of the dyes were almost the same.

Figure 3-5 (b) shows a comparison of the transient absorption kinetics of the dye cation in the DSSCs using the TBA electrolyte. Upon comparing the transient absorption kinetics between the Li electrolyte conditions and the TBA electrolyte conditions, no difference was observed for MK-1 and MK-88. For MK-31, when the Li^+ was replaced with TBA^+, the transient absorption kinetics was accelerated. However, this acceleration can be attributed to dye desorption. When the photo-electrode was filled with the TBA redox electrolyte, the MK-31 was slightly dissolved into the electrolyte. Therefore, this indicates that the counter cation ionic radius difference does not affect the regeneration.

The thickness of electric double layer on the semiconductor surface with the dye can be changed with the ionic radius of the counter cation[17]. When the TBA electrolyte was employed, the TBA cations in the electrolyte concentrated onto the donor moiety side of the dye. This is because TBA is too large to penetrate into the dye layer. Despite such electric double layer situations, the kinetics was not changed. Thus, from this result, it was expected that only the donor side HOMO contributed to the regeneration. Nevertheless the HOMO spread over the linker into the anchor side of the dye[18]. One reason why the anchor side orbitals did not contribute to the regeneration is the blocking effect against the approach of I^- by each dye. These dyes have alkyl chains that can block the approach of I_3^- to the semiconductor surface[19].

Therefore, the dyes will block not only I_3^- but also I^-. If alkyl chains block the I^-, the I^- electronic orbital is unable to reach the HOMO at the anchor moiety side. Additionally, the dyes were densely packed on the TiO_2 surface, which also contributed to the blocking of the approach of I^-.

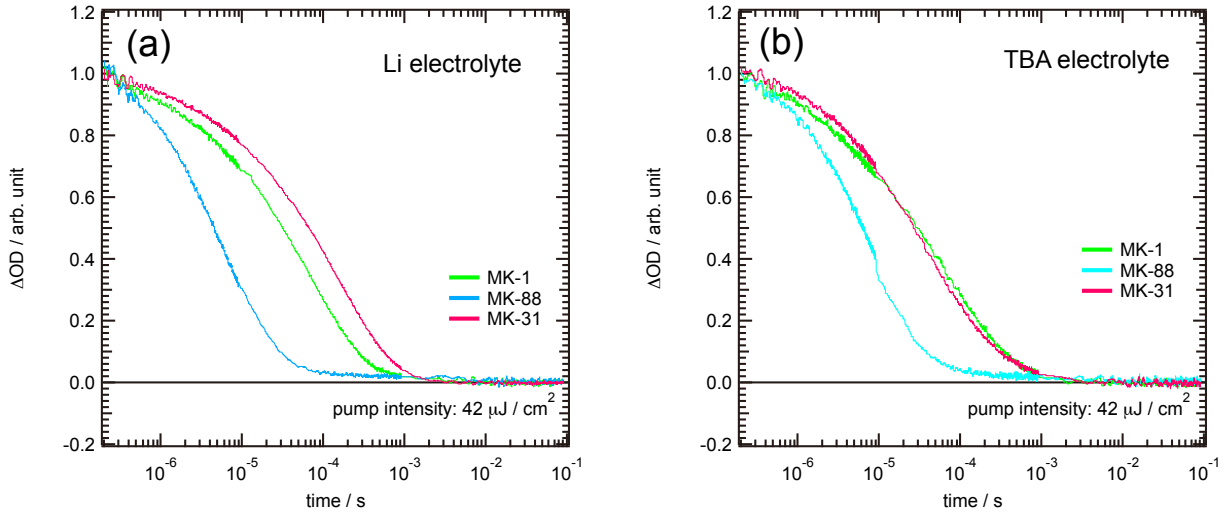

Figure 3-5. Comparison of transient absorption kinetics of the dye cation in DSSCs using different dyes. Dyes were MK-1, MK-88 and MK31. (a) Electrolytes were 0.3 M LiI, 0.05 M I_2 and 0.6 M *t*BP in acetonitrile. (b) Electrolytes were 0.3 M TBAI, 0.05 M I_2 and 0.6 M *t*BP in acetonitrile. Pump intensity was 42 $\mu J \cdot cm^{-2}$.

I employed the electronic coupling to explain the fastest regeneration rate of dye cation in DSSCs using MK-88 compared with that of the other dyes. Figure 3-6 shows HOMO of the dyes. The HOMO were calculated by Gaussian 09 with B3LYP/6-31G(d) level. The alkyl chains were removed in the calculation to calculate simply. The HOMO of MK-88 was larger at the donor moiety side than that of the other dyes. This larger HOMO of MK-88 could accelerate the regeneration rate. This is because large electronic coupling between HOMO and I^- can be expected.

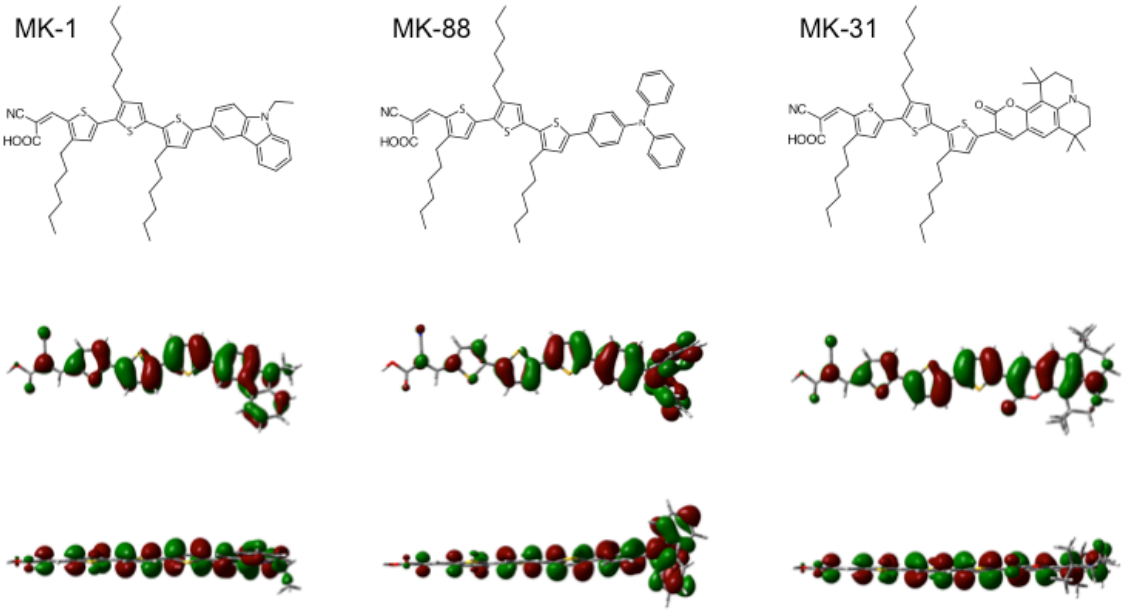

Figure 3-6. HOMO of the dyes. The HOMO were calculated by Gaussian 09 with B3LYP/6-31G(d) level. The alkyl chains were removed in the calculation to calculate simply.

To examine whether the electronic coupling affects the regeneration kinetics, the transient absorption kinetics was measured under reduced dye loading conditions. Figure 3-7 shows the transient absorption kinetics for MK-1 and MK-31. The adsorption densities were reduced to 44% for MK-1 and reduced to 22% for MK-31. When the adsorption density was reduced, the transient absorption kinetics was accelerated for both dyes. These results indicate that the sterically-bulky HOMO of the triphenylamine dyes contributed the dye regeneration. The effect of the adsorption density on the regeneration kinetics was larger than that of the free energy difference of 200 meV derived from the HOMO level difference between the dyes.

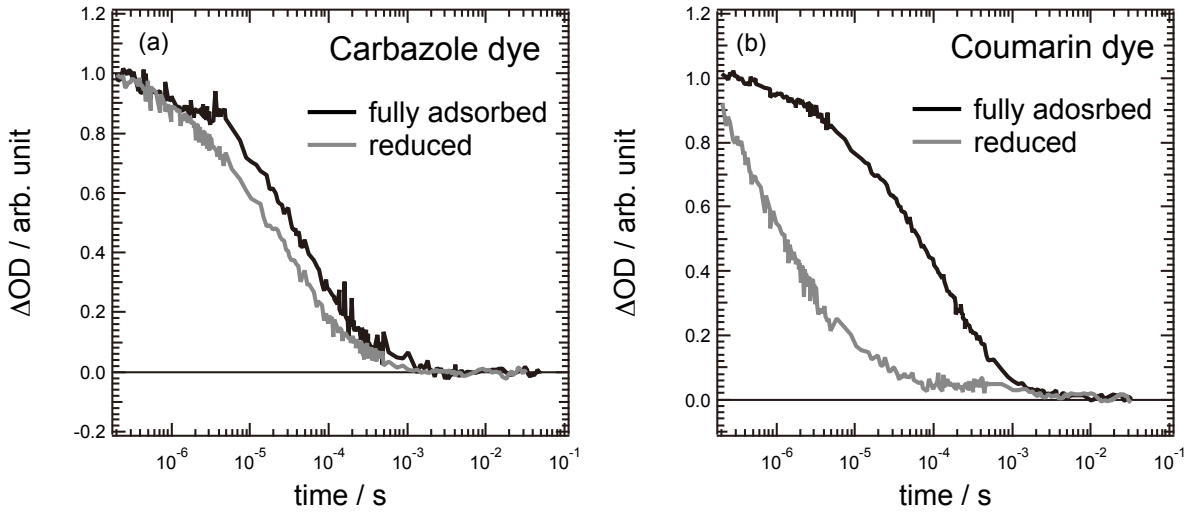

Figure 3-7. Transient absorption kinetics of the dye cation. (a) Adsorption density of dye MK-1 was controlled; (black line) full dye loading, (gray line) dye loading was reduced to 44%. (b) Adsorption density of dye MK-31 was controlled; (black line) full dye loading, (gray line) dye loading was reduced to 22%. Electrolytes were 0.3 M LiI, 0.05 M I_2 and 0.6 M *t*BP in acetonitrile. Pump intensity was 61 $\mu J \cdot cm^{-2}$.

The transient absorption kinetics of the DSSCs with MK-1 were similar to those with MK-31, even though the reaction free energy was different by approximately 200 meV. A previous study reported that the partial charge of the coumarin moiety attracted I_3^- through Li^+ in the electrolyte[19]. Likewise, it can be considered that the partial charge of coumarin moiety attracts I^-, which would affect the regeneration. To examine the attraction effect of the partial charge on the regeneration kinetics, electrolytes with different I^- concentrations were employed for the transient absorption measurements. If the coumarin moiety attracted I^- to the dye, the concentration dependence of I^- should be small.

Figure 3-8 shows the transient absorption kinetics of the dye cations of MK-1 and MK-31, respectively. The transient absorption kinetics decreased with the lower I^- concentration in the electrolyte. The differences for MK-1 and MK-31 were 3.5 and 2.8 times, respectively. Thus, the rate of the change of the transient absorption kinetics with MK-31 was slightly smaller than those for MK-1. Therefore, the attraction effect by the coumarin moiety may be suggested. In this measurement, these kinetics were not changed by repeat for each samples. The half time differences converged 10%.

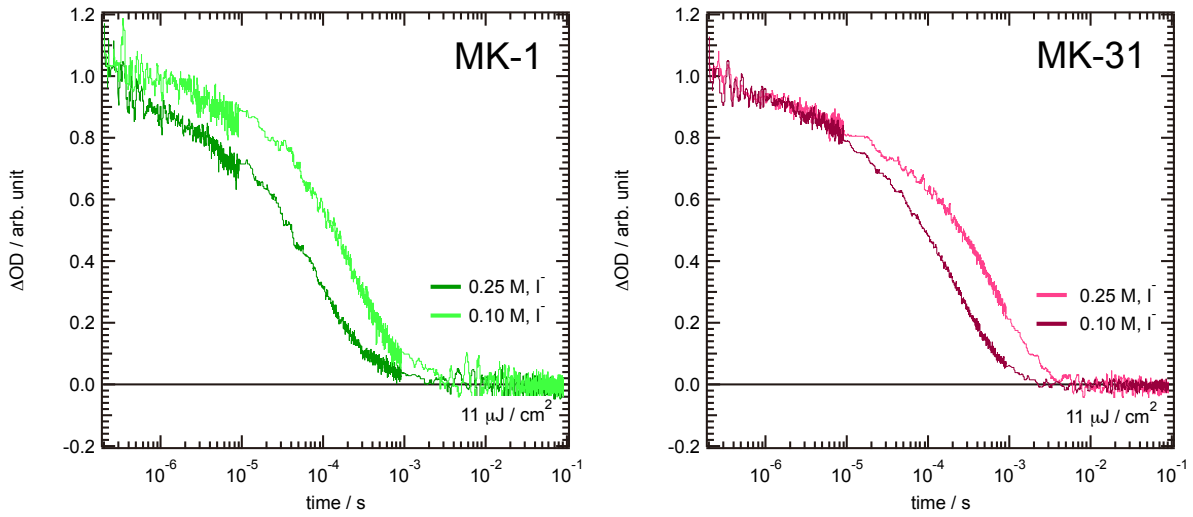

Figure 3-8. Transient absorption kinetics of the dye cation of (a) MK-1 and (b) MK-31. I^- concentration was controlled. Electrolytes were 0.3 M LiI, 0.05 M I_2 and 0.6 M *t*BP in acetonitrile (0.25 M, I^-) or 0.15 M LiI, 0.05 M I_2 and 0.6 M *t*BP in acetonitrile (0.10 M, I^-). Pump intensity was 11 $\mu J \cdot cm^{-2}$.

3-3-4. Recombination kinetics of dye cation

Figure 3-9 shows the recombination kinetics of dyes in the cells using inert electrolyte with Li cation as counter cation (a) and that of using inert electrolyte with TBA cation as counter cation (b). The energy difference between the conduction band edge of TiO_2 electrode and the HOMO level of the dye (ΔG) was changed by using different HOMO level dyes. The ΔG difference between DSSCs using MK-1 and those using MK-31 was approximately 200 meV. Nevertheless, the recombination kinetics were the same at the low electron density in the semiconductor electrode. The conduction band edge shift also did not affect the recombination. The conduction band edge was shifted with the replacement of the counter cation from Li^+ to

TBA^+. These results show that ΔG was a minor factor in the recombination kinetics. A little difference of a rate of change with the recombination kinetics to the pump intensity was observed between different of counter cations. The rate of change did not increased despite of the ΔG was enlarged. This result may suggest that interfacial electron transfer kinetics was controlled by invited region of Marcus theory.

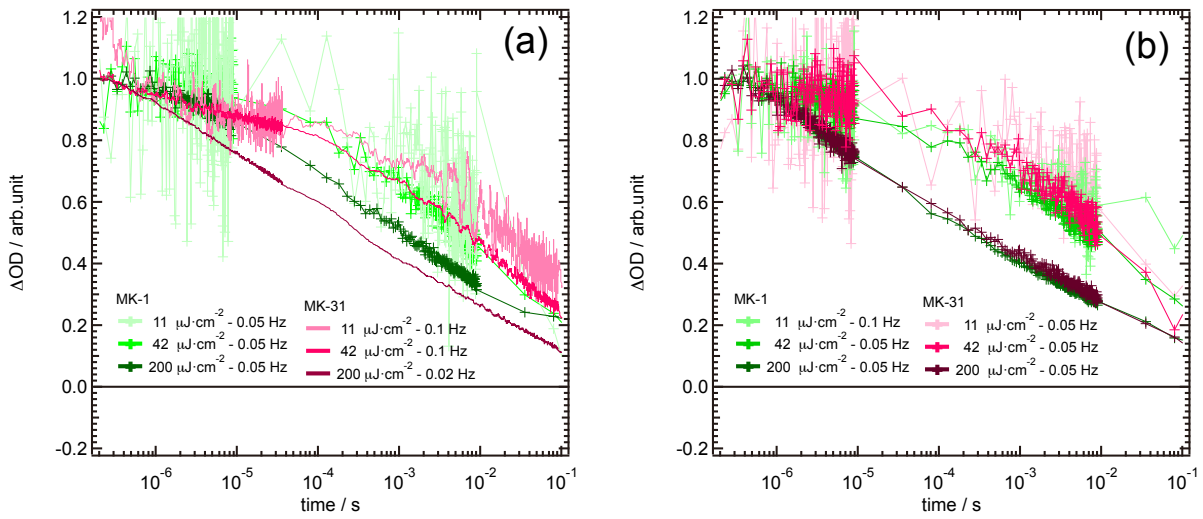

Figure 3-9. Transient absorption kinetics of the dye cation of DSSCs using different electrolytes. The pump intensities were 11, 42, and 200 μJ·cm^{-2}. The probe laser wavelength was 785 nm, the pump laser wavelength was 532 nm. The excitation frequency was decreased until the all injected electrons were recombined. (a) Electrolytes were 0.3 M $LiClO_4$ and 0.6 M *t*BP in acetonitrile. The pulse frequency for MK-1 was 0.05 Hz, and that for MK-31 was 0.1 or 0.02 Hz. (b) Electrolytes were 0.3 M $TBAClO_4$ and 0.6 M *t*BP in acetonitrile. The pulse frequency for MK-1 was 0.1 or 0.05 Hz, and that for MK-31 was 0.05 Hz.

3-4. Conclusions

Effects of the structure of the donor moiety on dye cation reduction kinetics were evaluated in the system of DSSCs with a D-π-A type metal-free organic dye. The donor structure difference of the dye was negligible impact to the recombination kinetics. On the other hand, the regeneration kinetics was affected by the donor structure difference. The electronic coupling effect was stronger than the free energy difference of 200 meV. When the HOMO was closely located by each adsorbed dye on TiO_2 surface, the electronic coupling between I^- and the HOMO was decreased, and thus the regeneration rate was decreased. Therefore, introduction of the sterically-bulky HOMO to the donor of the dyes so that the orbital faces bulk electrolyte is key strategy to obtain the high regeneration efficiency.

3-5. References

1 S. M. Feldt, G. Wang, G. Boschloo, A. Hagfeldt, *J. Phys. Chem. C*, 2011, **115**, 21500-21507.

2 G. Oskam, B. V. Bergeron, F. J. Meyer, P. C. Searson, *J. Phys. Chem. B*, 2001, **105**, 6867-6873.

3 B. A. Gregg, F. Pichot, S. Ferrere, C. L. Fields, *J. Phys. Chem. B*, 2001, **105**, 1422-1429.

4 Z. Zhang, P. Chen, T. N. Murakami, S. M. Zakeeruddin, M. Grätzel, *Adv. Funct. Mater.*, 2008, **18**, 341-346.

5 S. Wenger, P.-A. Bouit, Q. Chen, J. Teuschir, D. D. Censo, R. Humphry-Baker, J.-E. Moser, J.

L. Delgado, N. Martín, S. M. Zakeeruddin, M. Grätzel, *J. Am. Chem. Soc.*, 2010, **132**, 5164-5169.

6 S. M. Feldt, G. Wang, G. Boschloo, A. Hagfeldt, *J. Phys. Chem. C*, 2011, **115**, 21500-21507.

7 T. Daeneke, A. J. Mozer, Y. Uemura, S. Makuta, M. Fekete, Y. Tachibana, N. Koumura, U. Bach, L. Spiccia, *J. Am. Chem. Soc.*, 2012, **134**, 16925-16928.

8 R. A. Marcus, N. Sutin, *Biochim. Biophys. Acta*, 1985, **811**, 265-322.

9 S. M. Feldt, P. W. Lohse, F. Kessler, M. K. Nazeeruddin, M. Grätzel, G. Boschloo, and A. Hagfeldt, *Phys. Chem. Chem. Phys.*, 2013, **15**, 7087–7097.

10 J. N. Clifford, E. Palomares, M. K. Nazeeruddin, M. Grätzel, J. Nelson, X. Li, N. J. Long, J. R. Durrant, *J. Am. Chem. Soc.*, 2001, 4, **126**, 5225-5233.

11 I. Montanari, J. Nelson, and J. R. Durrant, *J. Phys. Chem. B*, 2002, **106**, 12203–12210.

12 S. M. Feldt, P. W. Lohse, F. Kessler, M. K. Nazeeruddin, M. Grätzel, G. Boschloo, and A. Hagfeldt, *Phys. Chem. Chem. Phys.*, 2013, **15**, 7087–7097.

13 S. M. Feldt, P. W. Lohse, F. Kessler, M. K. Nazeeruddin, M. Grätzel, G. Boschloo, and A. Hagfeldt, *Phys. Chem. Chem. Phys.*, 2013, **15**, 7087–7097.

14 P. G. Johansson, A. Kopecky, E. Galoppini, and G. J. Meyer, *J. Am. Chem. Soc.*, 2013, **135**, 8331–8341.

15 T. N. Murakami, N. Koumura, M. Kimura, S. Mori, *Langmuir*, 2014, **30**, 2274-2279.

16 I. Montanari, J. Nelson, J. R. Durrant, *J. Phys. Chem. B*, 2002, **106**, 12203-12210.

17 S. Nakade, T. Kanzaki, W. Kubo, T. Kitamura, Y. Wada, S. Yanagida, *J. Phys. Chem. B*, 2005, **109**, 3480-3487.

18 M. Miyashita, K. Sunahara, T. Nishikawa, Y. Uemura, N. Koumura, K. Hara, A. Mori, T. Abe, E. Suzuki, S. Mori, *J. Am. Chem. Soc.*, 2008, **130**, 17874-17881; Supporting Information, S8.

19 M. Miyashita, K. Sunahara, T. Nishikawa, Y. Uemura, N. Koumura, K. Hara, A. Mori, T. Abe, E. Suzuki, S. Mori, *J. Am. Chem. Soc.*, 2008, **130**, 17874-17881

Chapter 4

Effects of the alkyl chains to the π-conjugated linker on dye cation reduction kinetics

Chapter 4. Effects of the alkyl chains to the π-conjugated linker on dye cation reduction kinetics

4-1. Introduction

The open circuit voltage of the DSSCs is directly affected by the electron lifetime until an injected electron is recombined with a redox couple[1, 2]. The electron lifetime of the DSSCs with metal-free organic dyes are typically shorter than that of the DSSCs with ruthenium complex dyes. Thus, the lower open circuit voltages of DSSCs with metal-free organic dyes are the reason for the shorter electron lifetime. In one study, the electron lifetime was increased by introduction of alkyl chains to a π-conjugated linker of metal-free organic dyes. The alkyl chains can block the redox couple from approaching the semiconductor surface[3]. On the other hand, for the regeneration, the concentration of the redox couple around the dyes is desired to be higher. It can be assumed that introduction of the alkyl chains decreases the regeneration kinetics. Thus, in this chapter, the effects of the introduction of alkyl chains on the reduction kinetics were examined. For confirmation of generality, two types of dye were used for this study.

4-2. Experimental

Figure 4-1 shows the structures employed in this study. MK-1 and MK-3 are carbazole dyes with and without alkyl chains, respectively. MK-31 and NKX-2697 are coumarin dyes with

and without alkyl chains, respectively. The synthesis schemes are provided in the literatures[4-6]. The HOMO levels of MK-1, MK-3, MK-31 and NKX-2697 are 1.1, 1.1, 0.85, and 0.88 V vs NHE, respectively, as measured by the cyclic voltammetry technique.

I-V curve, IPCE spectrum and transient absorption measurements were performed with DSSCs with those dyes. The I-V curve measurements were performed by a solar simulator under two different light intensity conditions (83 and 20 $mW \cdot cm^{-2}$).

The transient absorption kinetics of the dye cation were measured under the operating condition. The dyes were induced by a 7-ns-pulsed Nd:YAG laser. The electrolyte compositions were 0.3 M LiI, 0.05 M I_2 and 0.6 M *t*BP in acetonitrile (I_3^-/I^- electrolyte) or 0.3 M $LiClO_4$ and 0.6 M *t*BP in acetonitrile (inert electrolyte).

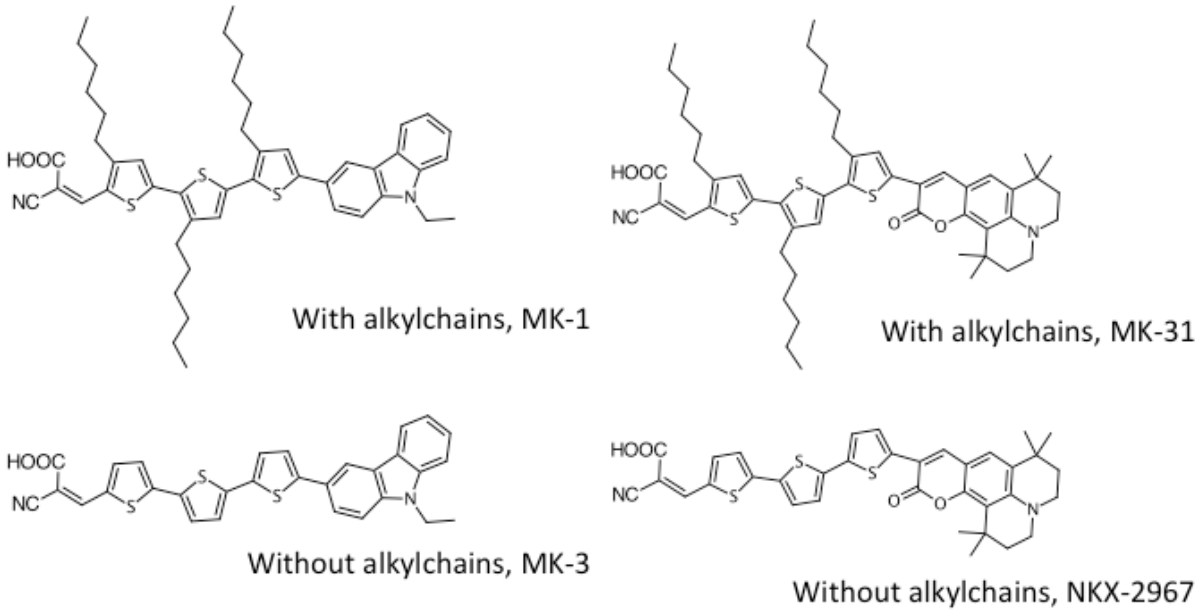

Figure 4-1. Molecular structures of carbazole dyes and coumarin dyes.

4-3. Results and Discussion

The reduction kinetics of the dye cations were evaluated after the measurements of I-V characteristic and IPCE spectra.

4-3-1. I-V characteristics and IPCE spectra

Figure 4-2 shows the I-V characteristics of carbazole dyes and coumarin dyes, respectively. The I_{sc} of each dye is proportional to the intensity of the solar simulator. This result indicates that the dye cations were immediately reduced by I^-. The V_{oc} of DSSCs using dyes with alkyl chains were higher than those without alkyl chains. This result was consistent with a previous study result[3]. The alkyl chains blocked the I_3^- from approaching the semiconductor surface. Figure 4-3 shows the IPCE spectra. The wavelength of the light selected as a pulsed pump laser, 532 nm, was absorbed by the dyes. By contrast, the wavelength of the light selected as the probe light, 785 nm, was negligibly absorbed by the dyes. Therefore, the dye cation reduction kinetics can be measured by the transient response measurement at 785 nm.

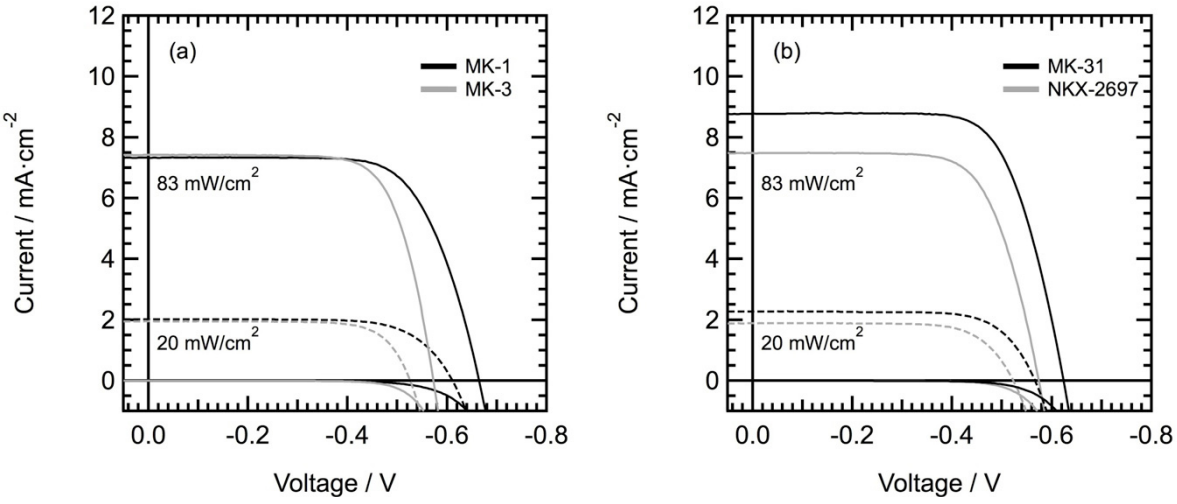

Figure 4-2. I-V curves of the DSSCs with MK-1 (black line) and MK-3 (gray line) (a); and with MK-31 (black line) and NKX-2697 (gray line) (b). The measured intensities under the solar simulator were 83 $mW \cdot cm^{-2}$ (solid line) and 20 $mW \cdot cm^{-2}$ (dashed line). The electrolytes were 0.3 M LiI, 0.05 M I_2 and 0.6 M *t*BP in acetonitrile.

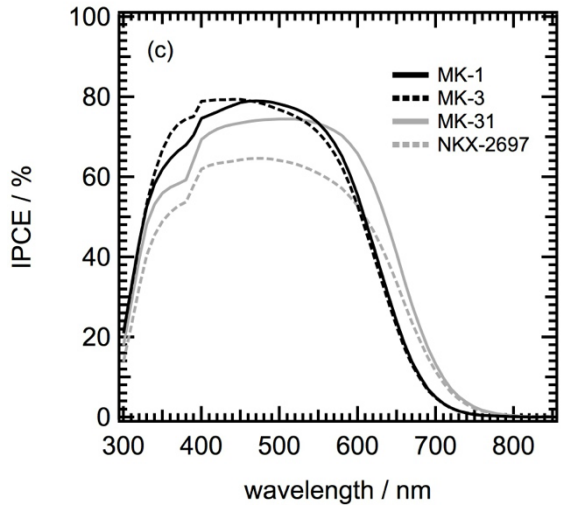

Figure 4-3. IPCE spectra. The black line shows the results of DSSCs with carbazole dyes. The gray line shows the results of DSSCs with coumarin dyes. The solid line and the dashed line are results of the dyes with and without alkyl chains. The electrolytes were 0.3 M LiI, 0.05 M I_2 and 0.6 M tBP in acetonitrile.

4-3-2. Effects of pump intensity on transient absorption kinetics of the dye cation

Figure 4-4 shows the transient absorption kinetics of the dye cation in an inert electrolyte. The transient absorption kinetics were measured under different intensities of the pulsed pump laser (30, 60, 90 and 150 $\mu J \cdot cm^{-2}$). The kinetics were compared by the half-times of the kinetic decay. Under every condition of the photo-electrodes, the transient absorption kinetics increased with the increasing intensity of the pulsed pump laser. This difference between 30 $\mu J \cdot cm^{-2}$ and 150 $\mu J \cdot cm^{-2}$ was approximately 10–20 times. This tendency was consistent with a previous result in which the recombination kinetics increased with increasing electron density in a semiconductor electrode[7].

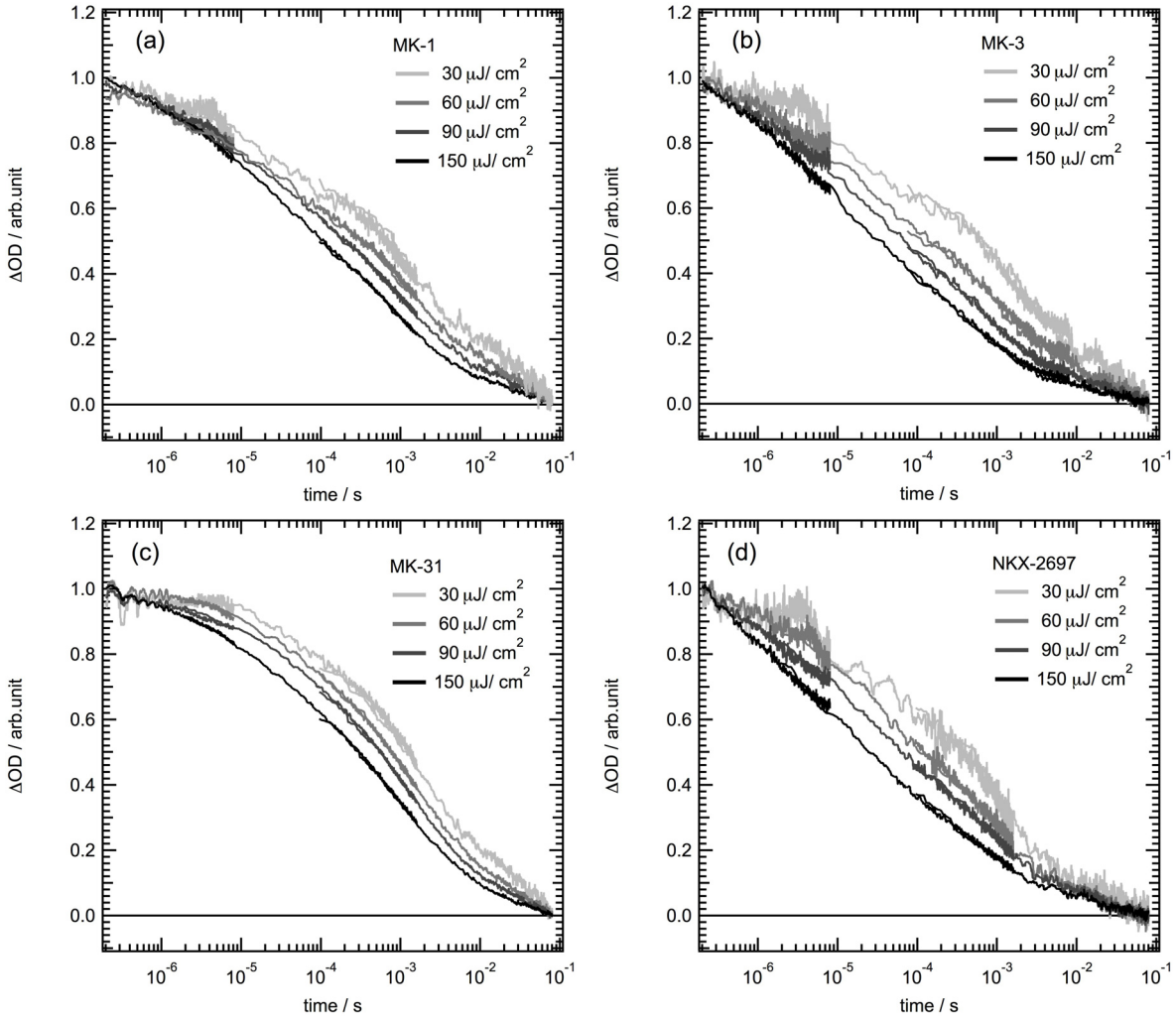

Figure 4-4. Transient absorption kinetics of a dye cation that adsorbed on a TiO_2 electrode. The dye cation was generated by electron injection from an excited state dye induced by a pulsed pump laser. Four intensities of the pulsed laser were used. The results are shown for (a) MK-1, (b) MK-3, (c) MK-31, and (d) NKX-2697. The electrolytes were 0.3 M $LiClO_4$ and 0.6 M *t*BP in acetonitrile.

4-3-3. Effects of alkyl chains of the dye on transient absorption kinetics of the dye cation

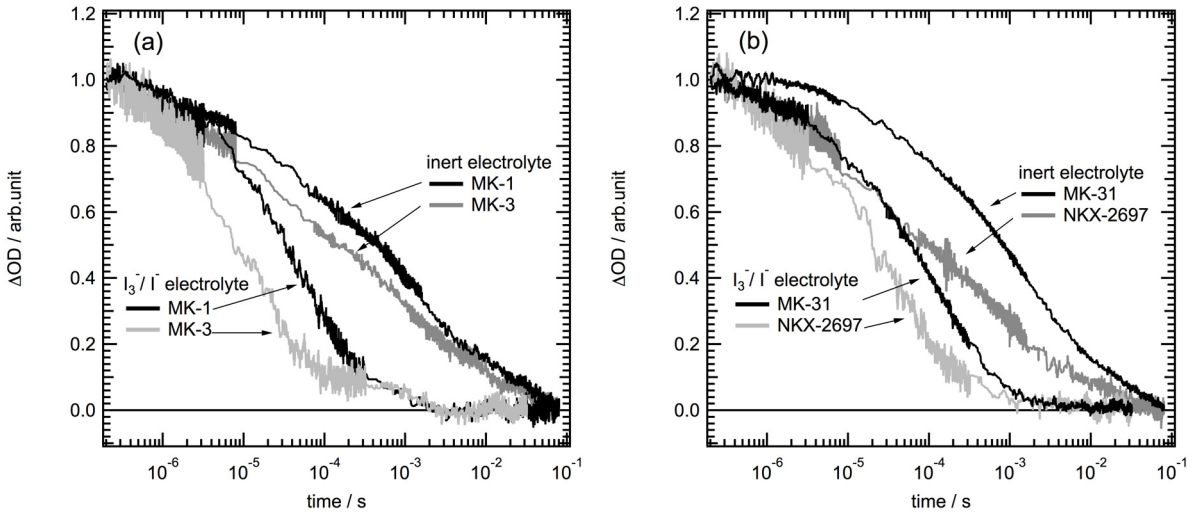

Figure 4-5. Transient absorption kinetics of the dye cation on DSSCs using (a) carbazole dyes or (b) coumarin dyes. The pulsed pump laser intensity was 60 μJ·cm^{-2}. The electrolytes were 0.3 M LiI, 0.05 M I_2 and 0.6 M *t*BP in acetonitrile (I_3^-/I^- electrolyte) or 0.3 M $LiClO_4$ and 0.6 M *t*BP in acetonitrile (inert electrolyte).

Figure 4-5 shows the transient absorption kinetics of the dye cation. Photo-electrodes were immersed in an I_3^-/I^- electrolyte or an inert electrolyte. The intensity of the pulsed laser was 60 μJ·cm^{-2}. Upon transient absorption kinetics measurement with an I_3^-/I^- electrolyte, the transient absorption kinetics were not changed when the intensity was changed in the range of 30–150 μJ·cm^{-2}, except when measured at 150 μJ·cm^{-2} with the coumarin dyes. These results indicate that the dye cation was mainly reduced by I^- in the I_3^-/I^- electrolyte. The half times of the transient absorption kinetics with the I_3^-/I^- electrolyte were approximately 10 times shorter than that those with the inert electrolyte. These results also indicate the higher regeneration rate of the

dye cation by I^-. This consideration is consistent with the I-V measurement results.

The transient absorption kinetics for both the I_3^-/I^- electrolyte and the inert electrolyte were decelerated by the introduction of the alkyl chains. This result was observed by DSSCs using both carbazole dye and coumarin dye. To examine the effect of alkyl chain introduction on the reduction kinetics, the effect on each factor of Marcus theory was discussed. The reduction kinetics can be written below:

$$\frac{d[dye^+]}{dt} = -k_1[dye^+][I^-] - k_2[dye^+][e_{CB}^-] \quad (4\text{-}1)$$

where k_i is the rate constant, t is the time, [dye^+] is the concentration of the dye cation, [I^-] is the concentration of I^- in the electrolyte, and [e^-] is the concentration of injected electrons in the semiconductor electrode. The rate constant can be written as:

$$k_i \propto \frac{2\pi}{\hbar}[H_{ab}]^2 \frac{1}{\sqrt{4\pi\lambda_i k_B T}} \exp[-\frac{(-\Delta G_i + \lambda_i)^2}{4\lambda_i k_B T}] \quad (4\text{-}2)$$

where H_{ab} is the electronic coupling between the electron donor and acceptor, and λ_i is the reorganization energy, which is the sum of the internal reorganization energy (λ_v) and the solvent reorganization energy (λ_s). ΔG_i is the free energy difference of reaction, k_B is the Boltzmann's constant, and T is the temperature[8]. ΔG_i was not changed by introduction of the alkyl chains. This is because the IPCE spectrum did not display a large difference upon the introduction of the

alkyl chains. The electrochemically measured HOMO levels were not changed by the introduction of the alkyl chains. The carbazole dye MK-1 and MK-3 HOMO levels were 1.06 and 1.05 V vs NHE, respectively, and the coumarin dye MK-31 and NKX-2697 HOMO levels were 0.85 and 0.88 V vs NHE, respectively. These results are consistent with the results of the IPCE spectrum measurements. The λ_i decreased with the introduction of alkyl chains. This is because when the alkyl chain is introduced, the molecular size is enlarged, leading to a reduction in the electric field received from solvent and an acceleration in the electron transfer kinetics. However, the transient absorption kinetics were decelerated by the introduction of the alkyl chains. Thus, this phenomenon cannot be explained by the reorganization energy difference. H_{ab} is affected by the distance between the electron donor orbital and the electron acceptor orbital. The introduced alkyl chains blocked I_3^- from approaching the semiconductor surface. This result is supported by the I-V results. Similarly, the introduced alkyl chains can block I^- from approaching the HOMO of the dyes. This is because alkyl chains do not contribute frontier orbitals. Therefore, the H_{ab} is deemed to be an effective factor to control the regeneration kinetics.

On the other hand, the transient absorption kinetics with an inert electrolyte (the recombination kinetics) cannot be explained by the electronic coupling between the TiO_2 surface and the HOMO of dye. The electronic coupling was not changed by introduction of the alkyl chains. This is because the orbital spreads up to the anchoring unit, and the dyes were vertically

adsorbed onto the TiO_2 surface. The adsorbed condition was estimated by DFT calculation[9] and measurement of the amount of dye. The measured amounts of the dyes decreased upon introducing the alkyl chains. Table 4-1 shows each molecular length from the carboxylic acid to the donor moiety, amount of adsorbed dyes and occupied areas on the TiO_2 electrode surface. The adsorption densities of the dye without alkyl chains are higher than that of the dye with alkyl chains, and the occupied area of the dye without alkyl chains are less than 1 nm^2. The lengths of the dyes are approximately 2 nm. Therefore, the adsorbed dyes are estimated to be standing.

Table 4-1. Amount and occupied area of dyes on TiO_2 electrode surface, and molecular length of dyes.

Dye	Alkyl chains	molecular length/ nm	Amount of dye/ 10^4 mol·cm^{-3}	Occupied area/ nm^2
MK-1	with	2.3	2.2	1.0
MK-3	without	2.3	5.4	0.4
MK-31	with	2.5	1.4	2.2
NKX2697	without	2.5	2.2	1.0

To explain these recombination kinetics, the hole transfer rate of the dyes was taken

into account. Typically, when the electron density was the same, the collision frequency between electrons in the conduction band of the semiconductor electrode and the dye cation should also be same because the diffusion coefficient of the electron is the same. When hole transfer occurs though, the collision frequency can be accelerated. This hypothesis is supported by the dense adsorption of the dyes.

4-3-4. Effect of hole transfer on the recombination kinetics

If the hole transfer rate affects the recombination kinetics of the dye cation, the recombination kinetics should decrease with decreasing adsorption density of the dyes. Photo-electrodes, whose adsorbing dyes were decreased by coadsorption with CDCA, were prepared for measurement of the recombination kinetics. Figure 4-6 shows the transient absorption kinetics of the dye cation with or without coadsorbed CDCA on the TiO_2 electrode in the inert electrolyte. The amounts of adsorbed dyes MK-1 and MK-3 were reduced to approximately 1/3 and 1/2 by coadsorption of the CDCA, respectively.

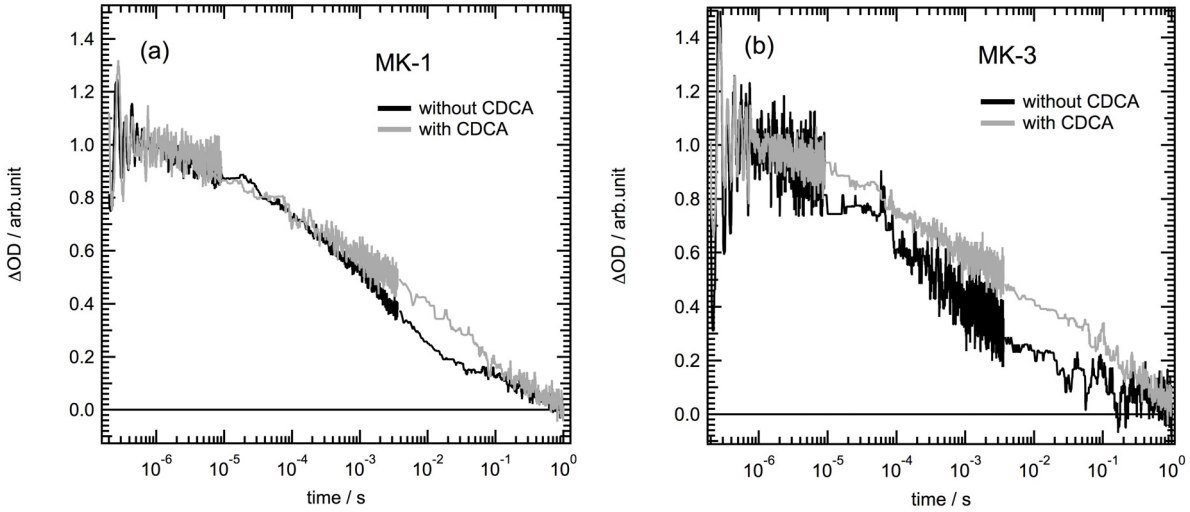

Figure 4-6. Transient absorption kinetics of the dye cation with or without coadsorbed CDCA on a TiO_2 electrode. (a) Carbazole dyes with alkyl chains, MK-1. Amount of adsorbed dye was reduced to approximately 1/3 by coadsorption of the CDCA. (b) Carbazole dye without alkyl chains, MK-3. Amount of adsorbed dye was reduced to approximately 1/2 by coadsorption of the CDCA. The pulsed pump laser intensity was 66 $mJ \cdot cm^{-2}$. The electrolytes were 0.3 M $LiClO_4$ and 0.6 M tBP in acetonitrile.

The transient absorption kinetics of the dye cation of MK-1 did not change with the decreasing amount of dye. On the other hand, the transient absorption kinetics of the dye cation of MK-3 did decrease with the decreasing amount of dye, becoming close to the kinetics of the dye cation of MK-1. These results indicate that the hole transfer rate affects the recombination kinetics of the dye cation. Values of the hole diffusion coefficient between dyes adsorbed on TiO_2 have been reported[10] on the order of 10^{-8} to 10^{-7} $cm^2 \cdot s^{-1}$. Values of the apparent diffusion coefficient of the electrons in a TiO_2 nanoporous electrode were on the order of 10^{-8} to 10^{-4} $cm^2 \cdot s^{-1}$. The values depend on electron density in the TiO_2 electrode. Thus, when the electron density is low, hole diffusion can affect the recombination kinetics.

4-4. Design guide of Dye structure

Introduction of the alkyl chains to the dye reduced the regeneration rate by decreasing the electronic coupling between dyes and I^-. To overcome a tradeoff between the electron lifetime and the regeneration kinetics caused by introduction of space separative substituent, the substituent should not be introduced to donor moiety side. The recombination kinetics were increased with hole hopping between dyes that is occurred by dense adsorption of dye. To avoid hole hopping, introduction of the space separative substituents to dyes, or the coadsorption into between dyes is required.

4-5. Conclusions

The introduction of alkyl chains to the π-conjugated linker retarded the regeneration kinetics and the recombination kinetics of the dye cation. The regeneration kinetics of the dye cation were more strongly affected by the electronic coupling between the HOMO of the dye and I^- than the reorganization energy. It was indicated that the recombination kinetics of the dye cation were affected by hole hopping between dyes. Introduction of alkyl chains reduced the hole hopping frequency. As a result, collisions between electrons in the TiO_2 and the dye cations were decreased, reducing the recombination kinetics. The design of sensitizing dye requires blocking the approach of I_3^- without interfering with I^- approaching the HOMO of the dye to obtain a higher regeneration efficiency with a longer electron lifetime.

4-6. References

1 A. Hagfeldt, G. Boschloo, L. Sun, L. Kloo, H. Pettersson, *Chem. Rev.*, 2010, **110**, 6595-9993.

2 M. J. Griffith, K. Sunahara, P. Wagner, K. Wagner, G. G. Wallace, D. L. Officer, A. Furube, R. Katoh, S. Mori, A. J. Mozer, *Chem. Commun.*, 2012, **48**, 4145-4162.

3 M. Miyashita, K. Sunahara, T. Nishikawa, Y. Uemura, N. Koumura, K. Hara, A. Mori, T. Abe, E. Suzuki, S. Mori, *J. Am. Chem. Soc.*, 2008, **130**, 17874-17881.

4 N. Koumura, Z. S. Wang, S. Mori, M. Miyashita, E. Suzuki, K. Hara, *J. Am. Chem. Soc.,* 2006, **128**, 14256-14257.

5 K. Hara, Z. S. Wang, T. Sato, A. Furube, R. Katoh, H. Sugihara, Y. Dan-Oh, C. Kasada, A. Shinpo, S. Suga, *J. Phys. Chem. B,* 2005, **109**, 15476-15482.

6 T. N. Murakami, N. Koumura, M. Kimura, and S. Mori, *Langmuir*, 2014, **30**, 2274–2279.

7 I. Montanari, J. Nelson, J. R. Durrant, *J. Phys. Chem. B*, 2002, **106**, 12203-12210.

8 J. N. Clifford, E. Palomares, M. K. Nazeeruddin, M. Grätzel, J. Nelson, X. Li, N. J. Long, J. R. Durrant, *J. Am. Chem. Soc.*, 2004, **126**, 5225-5233.

9 M. Pastore, E. Mosconi, and F. De Angelis, *J. Phys. Chem. C*, 2012, **116**, 5965–5973.

10 D. Moia, V. Vaissier, I. Lopez-Duarte, T. Torres, M. K. Nazeeruddin, B. C. O'Regan, J. Nelson, P. R. F. Barnes, *Chem. Sci.*, 2014, **5**, 281-290.

Chapter 5

Methods of Electron Lifetime Measurements

Chapter 5. Methods of electron lifetime measurements

The electron lifetime of DSSCs is the charge recombination time between electrons injected into a semiconductor electrode and a redox couple and/or cationic state dye. The electron lifetime is an important factor in DSSCs because it directly affects the open circuit voltage value. The electron lifetime is strongly related to the diffusion coefficient in the semiconductor electrode. Therefore, the diffusion coefficient has also been measured along with the electron lifetime. To measure these factors, many measurement methods have been proposed[1–3]. To obtain valid measurements, the operator must understand the required conditions. Then, depending on the situation, development of novel measurement methods may also be required.

5-1. Required Conditions for SLIM-PCV Methods

The required conditions of the DSSCs for the electron diffusion coefficient and electron lifetime measurement using a SLIM-PCV method were evaluated. This method is postulated that the electron density is uniform throughout the semiconductor electrode. Effects of electron density difference inside the photo-electrode on the measured values were investigated, and proper conditions were clarified.

5-1-1. Introduction

Stepped light-induced transient measurements of photocurrent and voltage (SLIM-PCV) is one electron lifetime and electron diffusion coefficient in the semiconductor measurement method[4]. The lifetime is obtained from the time constant of an exponential function that is fitted to the transient response. Therefore, the measurement system and an interpretation are simple, and then measurement time is short compared to that of other systems. However, to obtain valid measurements, certain requirements are necessary to satisfy the boundary conditions of the differential equation of this method. Here, measurement conditions were quantitatively inspected to obtain accurate values for the electron lifetime and the diffusion coefficient.

Here, to examine how the electron density profile difference affects these measured values, the laser irradiating direction effects on the measured values were investigated. If non-uniform electron density profiles exist, the measured values appear different between the irradiating directions.

5-1-2. Experimental

DSSCs semiconductor electrodes were fabricated from TiO_2 paste (DSL 18NR-T, Dyesol) deposited on FTO glass by the squeeze method. The TiO_2 electrode thicknesses were

controlled by the number of spacer tapes on the FTO glass and the viscosity of the paste, which was controlled by dilution with ethanol. The sensitizing dyes that were selected were the ruthenium complex dye N719 (molar extinction coefficient, ε = 13300 $dm^3 \cdot mol^{-1}$ at 500 nm in NaOH aq) and the metal-free organic dye MK-2 (ε = 38500 $dm^3 \cdot mol^{-1}$ at 473 nm in chloroform). Electrolytes were 0.1 M LiI, 0.6 M 1,2-dimethyl-3-n-propylimidazolium iodide (DMPImI), 0.05 M I_2 and 0.5 M 4-*tert*-butylpiridine (*t*BP) in acetonitrile. The electron lifetime, the diffusion coefficient and the electron density were measured using the electron lifetime and diffusion measurement system (PDL-100, EKO Instruments). Laser diodes (wavelength 473 or 660 nm, Kikoh Giken Co., LTD) were used as the dye excitation laser.

The electron lifetime is obtained from transient voltage fitting by an exponential function. In the open circuit condition, electron density in the semiconductor electrode of DSSCs can be written by a differential function:

$$\frac{\partial n(x,t)}{\partial t} = D\frac{\partial^2 n(x,t)}{\partial x^2} + G(x,t) - R(x,t) \qquad (5\text{-}1)$$

where *D* is the diffusion coefficient in the semiconductor electrode, *G* is the generation rate of electrons from the excited state dye injection, *R* is the recombination rate, *x* is the distance from the transparent substrate, *and t* is the time. Then, when the dye is excited in the photo-electrode uniformly, the analysis becomes simple. This uniformly excited condition results in no electron

density difference at any position in the semiconductor electrode. In other words, the electron density profile in the thickness direction is uniform. Therefore, *D* can be ignored, and equation 5-1 transforms to equation 5-2 at steady state, as explained in chapter 1.

$$n = G\tau \tag{5-2}$$

The diffusion coefficient is calculated from the time constant τ_c, which is obtained by fitting the transient current to an exponential function. The equation is:

$$D = \frac{L^2}{2.77\tau_c} \tag{5-3}$$

where *L* is the thickness of the semiconductor electrode.

The electron density measurement is performed by the charge extraction method[5]. The procedure of the electron density measurement in the open circuit condition consists of three steps, the laser irradiation of the photo-electrode, satisfying the condition for the open circuit by applied bias by a potentiostat, and turning off the light and the applied bias simultaneously and recording the transient current. The electron density value is calculated by integrating the transient current.

Here, on the electron lifetime, the diffusion coefficient, and the electron density measurement; the absorbance of the photo-electrode affects those measured results. This is because a large absorbance may generate a non-uniform electron density profile in the

semiconductor electrode. If the non-uniform electron density profile occurs, the diffusion term in the equation 5-1 cannot be ignored. Then, the measured values lose the meaning as comparable value with the other condition of DSSCs. Additionally, on the diffusion coefficient measurement and the electron density measurement, the diffusion length is affected by the thickness of the semiconductor electrodes. If the thickness is longer than the diffusion length, not all of the electrons are extracted. Therefore, thinner thickness of the semiconductor electrode compared with the diffusion length should be chosen for these measurements. Figure 5-1 shows schematic representation of electron density profiles in TiO_2 electrodes.

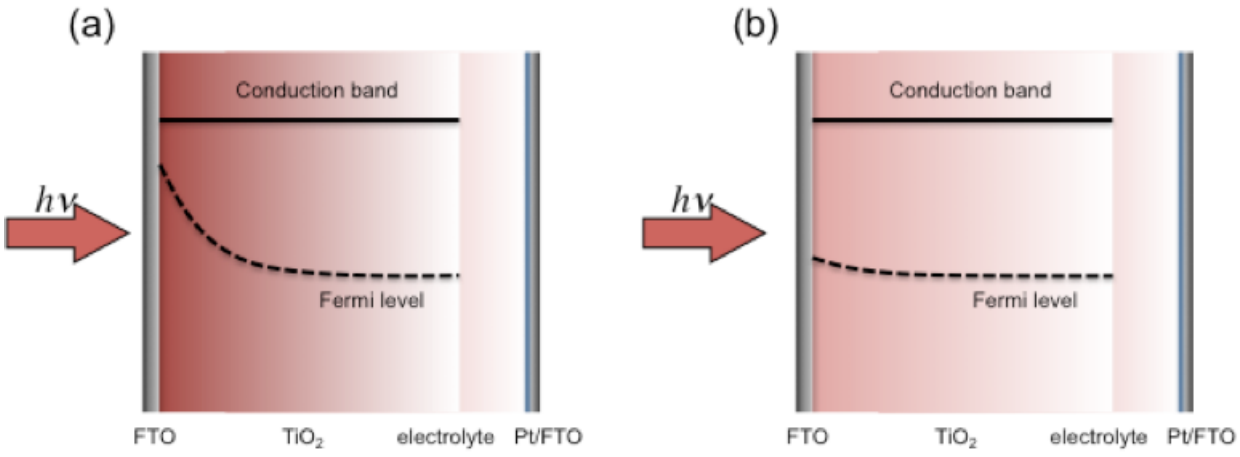

Figure 5-1. Schematic representation of electron density profiles in TiO_2 electrodes. TiO_2 electrode (a) with a high molar extinction coefficient dye at excitation light wavelength and (b) with a low molar extinction coefficient dye at excitation light wavelength.

5-1-3. Results and Discussion

Figure 5-2 shows the absorbance spectra of the photo-electrodes. The absorbance spectra have large differences between dyes even though their thicknesses were the same due to the molar extinction coefficient difference. The absorbance of the photo-electrode with MK-2 was over 3 with 3.6 μm thick photo-electrode. On the other hand, the absorbance of the photo-electrode with N719 did not reach 3 even with 20 μm thick photo-electrode. The absorbances at 473 and 660 nm also exhibit large differences between dyes. The absorbance at 473 nm was higher than that at 660 nm. Thus, a degree of uniformity difference between the wavelengths is expected.

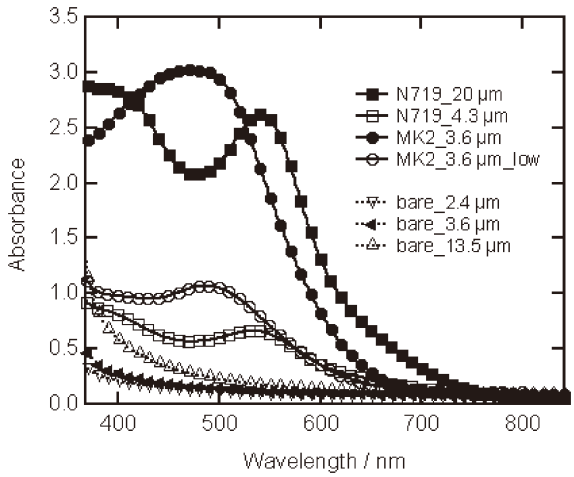

Figure 5-2. UV-vis spectra of photo-electrodes and bare electrodes. The thicknesses were employed over a range of 2.4–20 μm. Adsorbed dyes were N719 and MK-2. “low” denotes the condition for low adsorption density. “bare” denotes the condition of no dye adsorption.

Figure 5-3 shows the measured electron diffusion coefficients in DSSCs with various TiO_2 thicknesses. The laser wavelength was chosen to be 660 nm. The diffusion coefficients were not changed between irradiation to the photo-electrode side and the counter electrode side. The results indicate that the electron density profile in the semiconductor electrode was uniform. The absorbance of the photo-electrode with N719 at 660 nm was 0.6 and the thickness of the semiconductor electrode was 20 μm.

Figure 5-4 shows the measured electron diffusion coefficient in DSSCs with N719 or MK-2. Wavelengths of the excitation light were 473 or 660 nm. The thicknesses were ~3 μm. The absorbances of the photo-electrode with N719 and MK-2 at 473 nm were approximately 0.6 and over 3, respectively. The high absorbance of the photo-electrode with MK-2 indicates that the diffusion coefficient could not be measured correctly with the 473 nm laser irradiation.

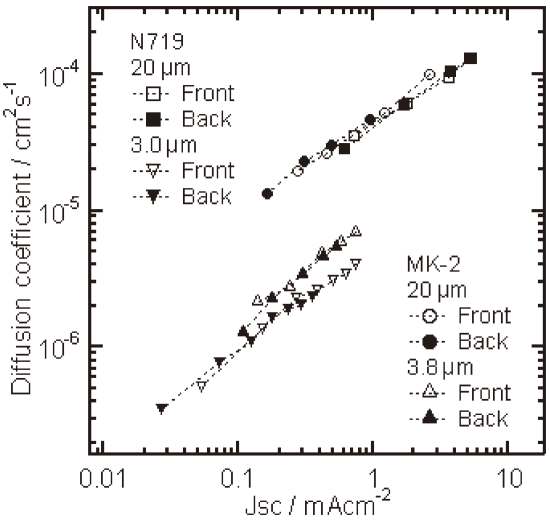

Figure 5-3. Measured electron diffusion coefficient in DSSCs with various TiO_2 thicknesses. Irradiation to photo-electrode side was denoted as "Front". Irradiation to counter electrode side was denoted as "Back". The laser wavelength was chosen to be 660 nm.

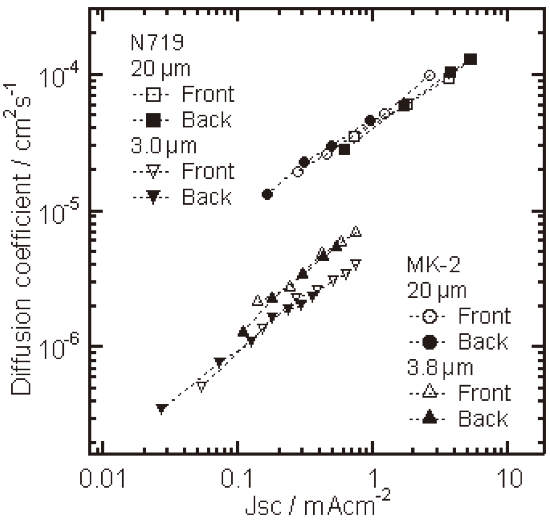

Figure 5-4. Measured electron diffusion coefficient in DSSCs. Wavelengths of excitation light were 473 and 660 nm. Irradiation to photo-electrode side was denoted as "Front". Irradiation to counter electrode side was denoted as "Back".

Figure 5-5 shows the transient currents with fitted results. The transient currents were measured from the photo-electrode side irradiation and the counter electrode side irradiation. The fitting was performed to an exponential function. The counter electrode side result was fitted exactly. On the other hand, the photo-electrode side was not fitted exactly. This result indicates the non-uniform electron density profile in the case of counter electrode side irradiation. To determine whether the different result between the two sides was affected by the non-uniform electron density profile with high absorbance, the amount of MK-2 that was reduced was also measured (Figure 5-6). Then, the values of the diffusion coefficient between the two sides were matched. The absorbance of the reduced dye photo-electrode was approximately 1. These examinations reveal that the diffusion coefficient was obtained correctly.

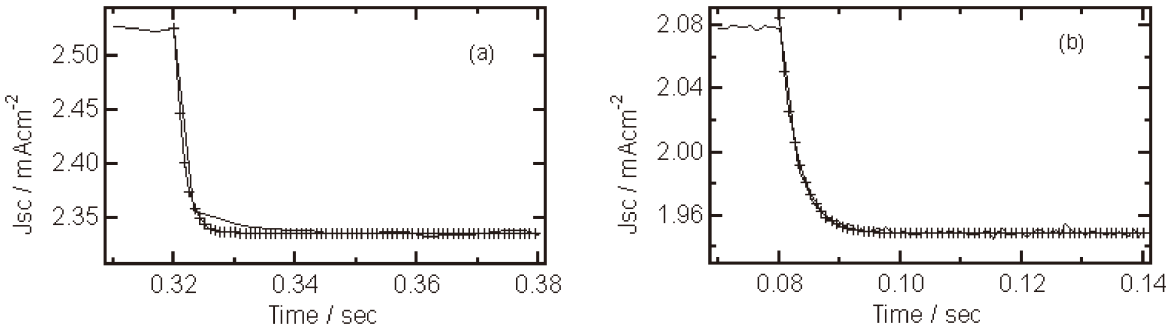

Figure 5-5. Transient current response in the short circuit condition. (a) Photo-electrode side irradiation, (b) Counter electrode side irradiation. The solid line stands for experimental results, and the line with symbols stand for the curve fitting result to an exponential function.

Figure 5-7 shows the measured electron lifetime of DSSCs prepared with N719. The TiO_2 thicknesses were 3.2 and 5.4 μm. The excitation laser wavelength was 635 nm. The DSSCs were irradiated from the photo-electrode side. This condition resulted in a uniform electron density profile, in which the electron lifetimes were matched. Next, the electron lifetimes were measured on the condition that the absorbance of the photo-electrode at the measured absorbance was over 3. The measurements were performed for both sides. The results are shown in Figure 5-8. The difference in the electron lifetime between the front side and the back side was not observed. The electron lifetime comparison between laser irradiation at 473 nm and that at 660 nm was also examined for the 20 μm thick semiconductor electrode with N719 (Figure 5-9). The absorbances at 473 and 660 nm were over 2 and less than 1, respectively, but the electron lifetime did not change.

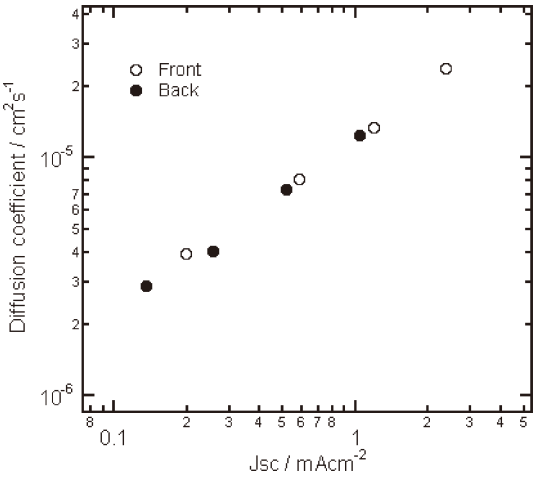

Figure 5-6. Measured electron diffusion coefficient of DSSCs prepared with a reduced amount of dye. Wavelength of excitation light was 473 nm. Irradiation to photo-electrode side is denoted as "Front". Irradiation to counter electrode side is denoted as "Back". The TiO_2 thickness was 3.6 μm. The dye was MK-2.

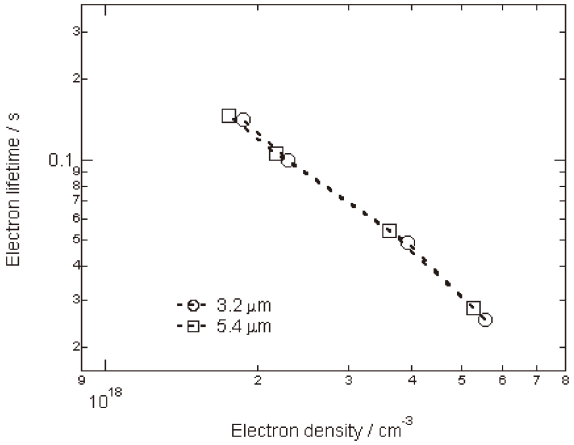

Figure 5-7. Measured electron lifetime of DSSCs prepared with N719. The TiO_2 thicknesses were 3.2 and 5.4 μm. Laser wavelength was 635 nm. The DSSCs were irradiated from the photo-electrode side.

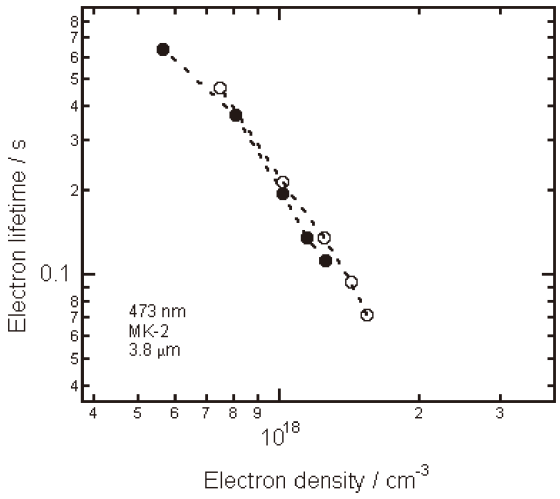

Figure 5-8. Measured electron lifetime of DSSCs prepared with MK-2. The TiO_2 thickness was 3.8 μm. Laser wavelength was 473 nm. The DSSCs were irradiated from the photo-electrode side (open symbol) and the counter electrode side (closed symbol).

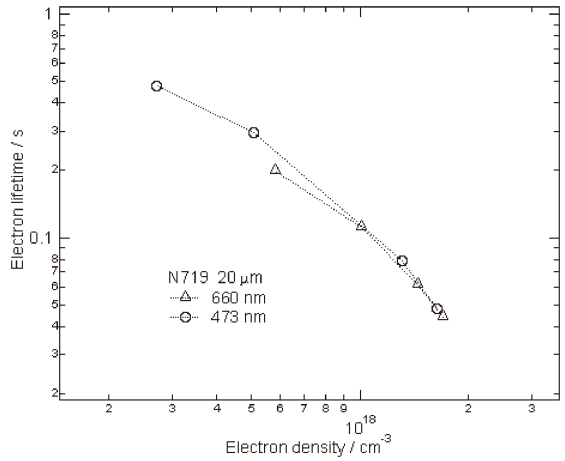

Figure 5-9. Measured electron lifetime of DSSCs prepared with N719. The TiO_2 thickness was 20 μm. The laser wavelength was set to 635 and 473 nm. The DSSCs were irradiated from the photo-electrode side.

5-1-4. Conclusions

The required conditions for the electron diffusion coefficient and the electron lifetime measurement were studied for various absorbances of the photo-electrode. The electron diffusion coefficient required a lower absorbance of the photo-electrode of less than 1. The electron lifetime was correctly obtained with a higher absorbance of approximately 3.

5-2. Development of a method to measure the electron lifetime in the dark

A novel electron lifetime measurement method for the DSSCs that is not required an electron injection from excited dyes was proposed. Validity of the electron lifetime measured by the novel method was evaluated by comparison of the electron lifetime measured by the SLIM-PCV method.

5-2-1. Introduction

In our laboratory, we predicted that electron lifetime measurement without light irradiation is an effective measurement for deep analysis of the DSSC electron transfer mechanism. This method can distinguish between the recombination kinetics of the two paths on the electron lifetime. Moreover, this method can measure the electron lifetimes on any interface condition of the semiconductor electrode. Therefore, to measure without light irradiation, a novel method, stepped current induced measurement of cell voltage in the dark (darkSCIM) was proposed. In the darkSCIM method, the electrons were injected from the FTO glass side by an external circuit. However, the validity of this darkSCIM method was not sufficiently verified. Therefore, to determine the validity of the darkSCIM method, electron lifetimes measured by darkSCIM were compared with electron lifetimes measured by SLIM-PCV.

5-2-2. Experimental

The DSSC semiconductor electrodes were fabricated from TiO_2 paste (Nanoxide-T, Solaronix) deposited on FTO glass by the squeeze method. The TiO_2 electrode thicknesses were controlled by the number of spacer tapes on the FTO glass and the viscosity of the paste. The thicknesses were 3.2, 5.4 and 8.2 μm. The TiO_2 electrodes were sintered at 450°C for 30 min. Photo-electrodes were obtained by immersing in the dye solution at 90°C overnight. N719 was chosen as the sensitizing dye and dissolved in mixed solvent (acetonitrile, AN : t-BuOH = 1 : 1) Electrolytes were 0.1 M LiI, 0.6 M 1,2-dimethyl-3-n-propylimidazolium iodide (DMPImI), 0.05 M I_2 and 0.5 M 4-*tert*-butylpiridine (*t*BP) in acetonitrile. Counter electrodes were Pt-spattered FTO glass.

In the darkSCIM method, a galvanostat (HABF-5001, Hokuto Denko) was used for electron injection into the semiconductor. The galvanostat was controlled by a PC with a digital-to-analog converter. A multimeter (AD7461A, Advantest) recorded the transient voltage of the DSSCs. Figure 5-10 shows a schematic representation of the darkSCIM method.

The electron density was measured by the charge extraction method[5]. Under the dark condition, the electron density was measured using the applied bias for electron injection and extraction when the bias was cut off. In this measurement, the porosity of the semiconductor electrode was not taken into account.

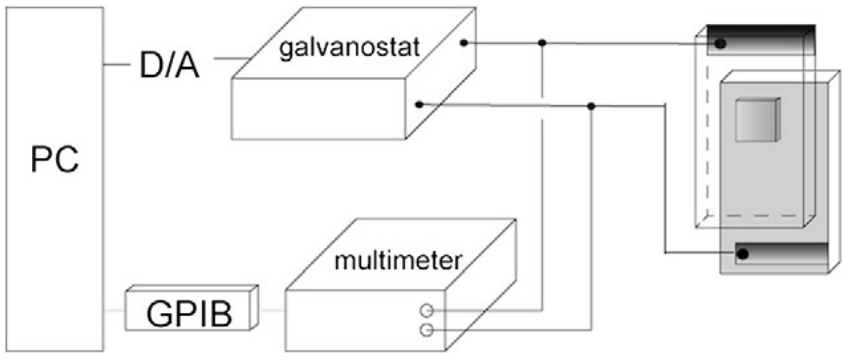

Figure 5-10. Schematic representation of the measurement system for stepped current-induced measurements of the DSSC cell voltage in the dark (darkSCIM). Electron injection into the semiconductor electrode was performed by the galvanostat. The galvanostat was controlled by a PC with a digital-to-analog converter. The multimeter records the transient voltage of the DSSCs.

5-2-3. Results and Discussion

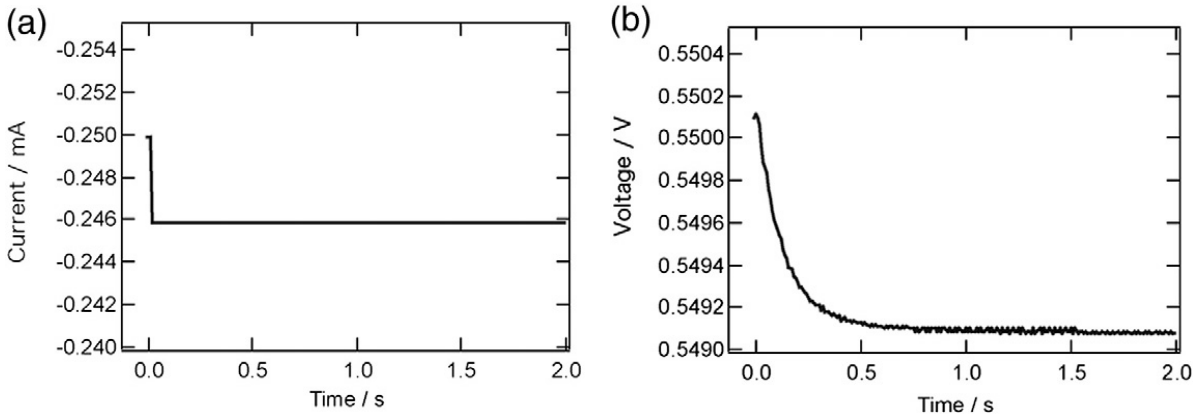

Figure 5-11. Measured (a) transient current and (b) transient voltage by darkSCIM.

Figure 5-11 shows an injected transient current and an observed transient cell voltage measured by the darkSCIM method. When the injected current was slightly decreased stepwise, the cell voltage was simultaneously exponentially decreased. Figure 5-12 shows the electron lifetime and the applied voltage as a function of the electron density. The electron lifetime at each thickness measured by darkSCIM was same as that measured by SLIM-PCV. An electron lifetime difference of the DSSCs between the 8.2 μm thick electrode and the other electrode thicknesses was observed and was attributed to less dye loading. An electron density difference between DSSCs with various thicknesses was not observed. Therefore, the same electron density profile in the semiconductor electrodes was indicated even though the electrons were injected from only the FTO side. The plot of voltage vs. the electron density showed a difference of approximately 40 mV at the same electron density between darkSCIM and SLIM-PCV due to the IR drop. The cell resistance multiplied by the injected current was consistent with this difference. The resistance was measured by impedance spectroscopy.

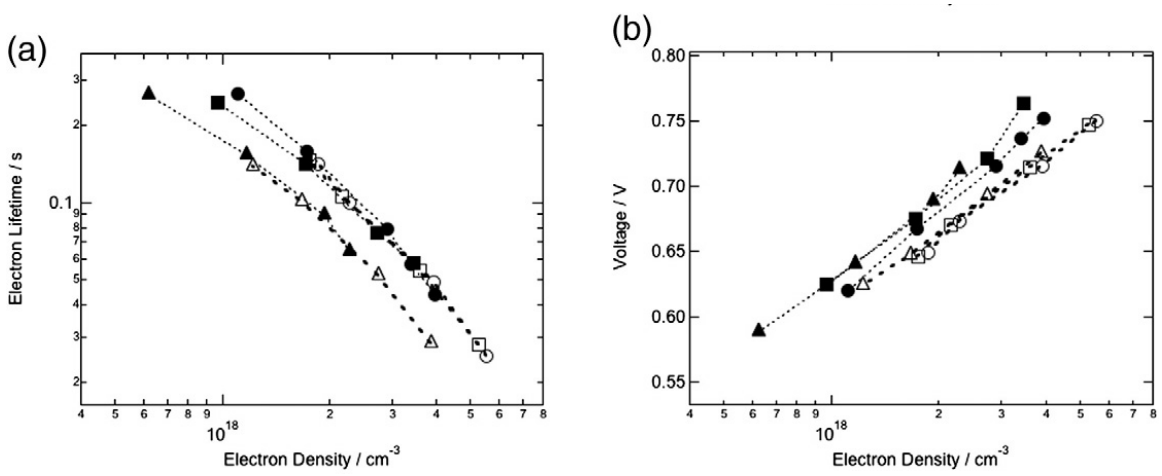

Figure 5-12. Measured (a) electron lifetime and (b) applied circuit voltage as a function of electron density. Open symbols were measured by darkSCIM; closed symbols were measured by SLIM-PCV. Circle, square, and triangle symbols stand for thicknesses of 3.2, 5.4 and 8.2 μm, respectively.

Figure 5-13 shows the electron lifetime comparison between DSSCs with N719 and those without dye. The electron lifetimes were measured by the darkSCIM method. At the same electron density, the electron lifetime with N719 was approximately 5 times longer than without the dye. This result clearly shows the I_3^- blocking effect[6] of the adsorbed dye.

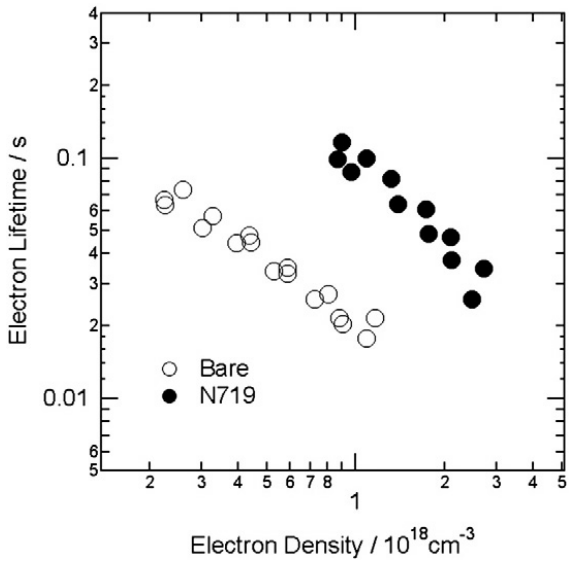

Figure 5-13. Measured electron lifetime by the darkSCIM method. Open symbols represent the no dye-adsorbed condition (Bare). Closed symbols are DSSCs with N719.

5-2-4. Conclusions

A novel electron lifetime measurement method of DSSCs, darkSCIM, was proposed. The darkSCIM method does not require the injection of electrons from an excited dye. The electrons were injected from the FTO glass side by an external circuit. In this method, the validity was confirmed by comparison with the SLIM-PCV method. By this darkSCIM method, the electron lifetimes of DSSCs were measurable under the following conditions: the DSSCs use a dye with a low electron injection efficiency; the DSSCs use a dye that absorbs negligible visible light; the DSSCs using a semiconductor electrode that adsorbs only coadsorbent; and the DSSCs use bare semiconductor electrodes.

5-3. References

1 G. Schlichthörl, S. Y. Huang, J. Sprague, and A. J. Frank, *J. Phys. Chem. B*, 1997, **101**, 8141-8155.

2 L. Dloczik, O. Ileperuma, I. Lauermann, L. M. Peter, E. A. Ponomarev,

G. Redmond, N. J. Shaw, and I. Uhlendorf, *J. Phys. Chem. B*, 1997, **101**, 10281-10289.

3 J. Bisquert, *J. Phys. Chem. B*, 2002, **106**, 325-333.

4 S. Nakade, T. Kanzaki, Y. Wada, and S. Yanagida, *Langmuir*, 2005, **21**, 10803-10807.

5 N.W. Duffy, L. M. Peter, R. M. G. Rajapakse, K. G. U. Wijayantha, *Electrochemistry Commiunications*, 2000, **2**, 658-662.

6 T. Abe, E. Suzuki, S. Mori, *J. Am. Chem. Soc.*, 2008, **130**, 17874-17881.

Chapter 6

Effects of the Molecular Structure of the Dye on the Electron Lifetime

Chapter 6. Effects of the molecular structure of the dye on the electron lifetime

Electron lifetime is an important factor in determining the open circuit voltage of DSSCs. The electron lifetime is strongly affected by differences in the molecular structure of the dye[1]. One of the effective factors of the electron lifetime is the local concentration of I_3^- near the semiconductor electrode surface. Control of the local concentration of I_3^- can be performed by a molecular engineering approach that focuses on the blocking, the partial charge, and the dispersion force[2]. In this chapter, these effect on the electron lifetime was evaluated.

6-1. Effect of the introduction of a non π-conjugated moiety into the anchoring unit of a D-π-A type organic dye on the electron lifetime

6-1-1. Introduction

Since the first dye-sensitized solar cells was reported by Grätzel et al., metal complex dyes have been selected for high power conversion efficiency DSSCs. Ruthenium, which is a rare metal, has generally been selected as the central metal of the metal complex dyes[3–5]. An advantage of the DSSCs their expected low-cost production. To obtain this advantage sufficiently, a metal-free organic dye is desired. DSSCs with metal-free organic dyes have also

been actively investigated, and their performances are analogous to those of DSSCs with metal complex dyes[6–9]. The organic dye can introduce structural variety by replacing or introducing substituents[3]. This structural variety enables the dyes to introduce functions. For example, introduced alkyl chains reducing the approach of I_3^- to the semiconductor surface[1]. However, due to the structural variety, the effects of differences in the dye molecular structure on the electron lifetime have not been studied systematically.

The power conversion efficiency of DSSCs is determined not only by the open circuit voltage but also by the short circuit current. Thus, the electron lifetimes have not yet sufficiently been measured on dye structures that are expected to have low I_{sc}. Investigations under the low performance condition are needed to obtain systematic information on the electron lifetime dependent on the structure of the dye. Hence, the effects of the addition of a non π-conjugated moiety into the anchor unit of a D-π-A type organic dye were examined. The non π-conjugated linker at the anchor unit may reduce the electronic coupling between the semiconductor surface and the LUMO of dye.

6-1-2. Experimental

DSSCs were prepared and characterized by the method described in chapter 2 of this thesis. Semiconductor porous electrodes were prepared from TiO_2 paste (Nanoxide-T, Solaronix). The thickness of the TiO_2 electrodes was ~3.5 μm. Electrolytes were 0.1 LiI, 0.6 M DMPImI,

0.05 M I_2 and 0.6 M tBP in acetonitrile. Carbazole dyes (MK-2, MKZ-35 and MKZ-36) were used as sensitizers. The structures are shown in Figure 6-1.

Fluorescence quenching experiments were performed as a function of quencher concentration. I_3^- was chosen as quencher and prepared by blending TBAI and I_2 at an equal ratio. The dyes were dissolved in mixed solvent (t-BuOH/AN/ toluene = 1:1:1 volume ratio) to a concentration of 0.01 mM.

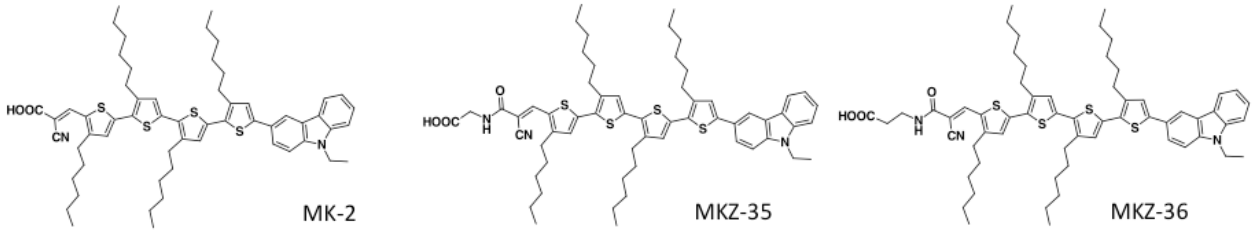

Figure 6-1. Structures of dyes. MK-2 was used as a reference. MKZ-35 and MKZ-36 have a non π-conjugated moiety (methylene unit) introduced between the carboxyl acid and cyano units.

6-1-3. Results and Discussion

i. I-V measurement

I-V characteristic results of the DSSCs using dyes (MK-2, MKZ-35 and MKZ-36) are shown below.

Table 6-1. I-V characteristics of DSSCs using dyes (MK-2, MKZ-35 and MKZ-36). The measured conditions under the solar simulator were 1 sun. The electrolytes were 0.1 M LiI, 0.6 M DMPImI, 0.05 M I_2, and 0.6 M *t*BP in acetonitrile.

Dye	Thickness/ μm	V_{oc}/ V	J_{sc}/ mAcm^{-2}	*FF*	*PCE*/%
MK-2	3.2	0.70	9.9	0.61	4.2
MKZ-35	3.5	0.75	8.7	0.65	4.3
MKZ-36	3.4	0.72	7.3	0.69	3.6

I_{sc} decreased in the order of MK-35 > MK-36 > MK-2. This result indicates lower electron injection efficiency upon addition of a methylene unit. On the other hand, V_{oc} increased with the addition of the methylene unit despite the decrease in I_{sc}. For that reason, DSSCs with MKZ-35 were expected to have the longest electron lifetime compared to those with other dyes. To examine the electron lifetimes quantitatively, SLIM-PCV and darkSCIM measurements were performed.

ii. Electron lifetime measurement

The electron lifetime and the open circuit voltage as a function of electron density are

shown in Figure 6-2. The open circuit voltages were almost the same at the same electron density between the dyes. The electron lifetime of DSSCs with MKZ-35 was the longest. The electron lifetime of the MKZ-36 system was the same as that of the MK-2 system. However, the open circuit voltage has approximately a 30 mV difference between the two dyes due to the time-dependent change. The electron lifetime usually decreases with increasing open circuit voltage at the same electron density derived from the potential negative shift of the semiconductor. Thus, this result was consistent with the I-V characteristics. In all dyes, the blocking effect of I_3^- by dye was observed by comparison with the bare electrode. Note that "bare" indicates the semiconductor electrode without dye adsorption.

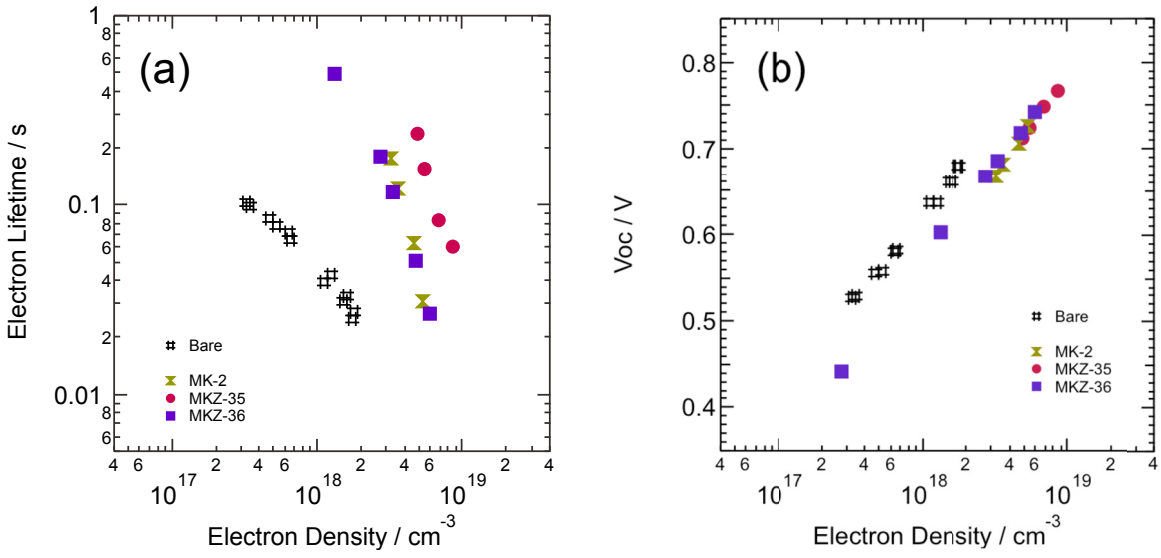

Figure 6-2. (a) Electron lifetime of DSSCs with dyes and without dye as a function of electron density. "Bare" is without dye, as measured by the darkSCIM method. (b) Open circuit voltage of DSSCs with dyes and without dye as a function of electron density. "Bare" is without dye, as measured by the charge extraction in the dark.

To examine the reason for the longer electron lifetime of the DSSCs with MKZ-35, electron lifetimes in the reduced dye condition were measured. In DSSCs using the D-π-A organic dyes, usually, not only the blocking effect but also the dispersion force affects the electron lifetime. Miyashita et al. reported that the electron lifetime with a D-π-A type organic dye was decreased relative to that of a bare electrode with a decreasing amount of adsorbed dye. The reason was attributed to I_3^- attraction by the dye molecule by dark current measurements[1]. Here, the dyes MK-2, MKZ-35 and -36 do not have large partial charges, and basic framework is the same as for the dyes that attract I_3^-. Therefore, these dyes will attract I_3^- by the dispersion force, which will decrease the electron lifetime. Figure 6-3 shows the electron lifetime and open circuit voltage of DSSCs with each dye as a function of the electron density. The electron lifetimes were decreased relative to the bare electrode upon decreasing the amount of dye. This result is consistent with a previous report. Thus, in this experiment, the results also indicate that the dyes attract I_3^- to the TiO_2 electrode surface.

The conditions of "reduced" denote that the amount of adsorbed dye was reduced up to approximately 10% compared with the condition of "full". Thus, the blocking effect was not expected. The electron lifetime of the "reduced" condition of MKZ-35 was approximately 10 times longer than that of MK-2 and MKZ-36 and was near the "bare" condition. Therefore, these results suggest that the attraction force of MKZ-35 is weak.

Table 6-2. I-V characteristics of DSSCs using dyes (MK-2, MKZ-35 and MKZ-36) full and with reduced condition of dye loading. The measured conditions under the solar simulator were 1 sun. The electrolytes were 0.1 M LiI, 0.6 M DMPImI, 0.05 M I_2, and 0.6 M *t*BP in acetonitrile.

Dye	Dye loading	Thickness/ μm	V_{oc}/ V	J_{sc}/ mAcm^{-2}	*FF*	*PCE*/ %
MK-2	full	3.2	0.70	9.9	0.61	4.2
MK-2	reduced 3%	3.3	0.50	1.7	0.73	0.6
MKZ-35	full	3.5	0.75	8.7	0.65	4.3
MKZ-35	middle 30%	3.2	0.60	5.4	0.74	2.4
MKZ-35	reduced 8%	3.2	0.59	2.7	0.76	1.2
MKZ-36	full	3.4	0.72	7.3	0.69	3.6
MKZ-36	middle 40%	3.5	0.58	4.4	0.68	1.7
MKZ-36	reduced 5%	3.1	0.49	1.2	0.71	0.4

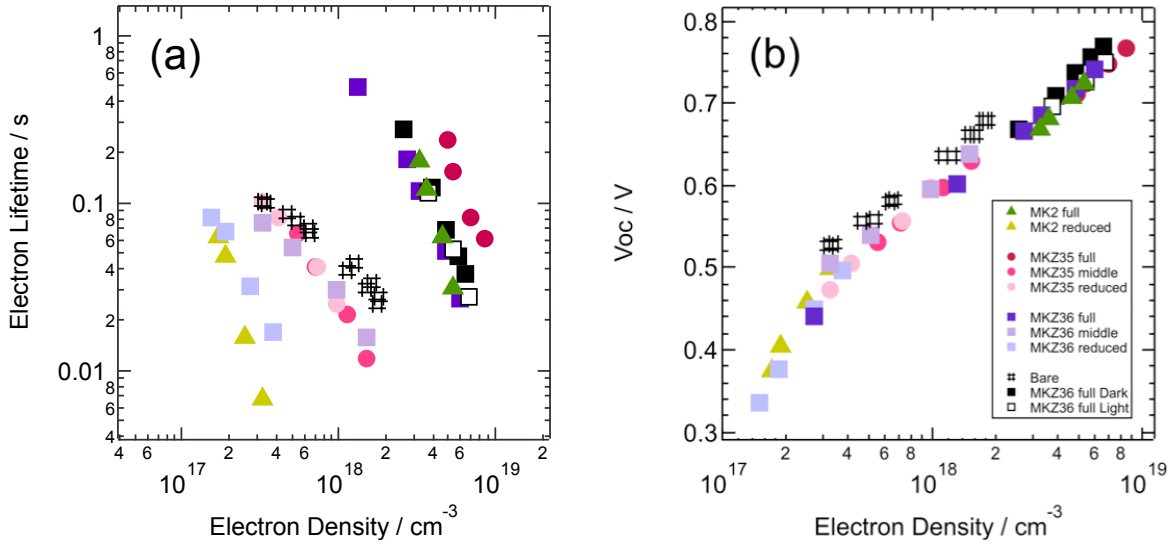

Figure 6-3. (a) Electron lifetime of DSSCs with full and reduced amounts of dyes as a function of electron density. "Bare" and "Dark" were measured by the darkSCIM method, which does not use light irradiation for electron injection from the excited state dye into the conduction band of the semiconductor. (b) Open circuit voltage of DSSCs with full and reduced amounts of dyes as a function of electron density. "Bare" and "Dark" were measured by the charge extraction method in the dark.

iii. Fluorescence quenching experiment

To directly observe the I_3^- attraction force difference, a fluorescence quenching experiment was employed. Figure 6-4 shows the fluorescence quenching of dyes by I_3^-. The vertical axis is the ratio of fluorescence intensity (I_F^0/I_F). I_F^0 and I_F are the fluorescence intensities without and with a fluorescence quencher, respectively[10]. The fluorescence intensities were decreased with increasing I_3^- concentration in the dye solution. This result was consistent

with a report by Splan et al[11]. Thus, the dyes would be quenched by I_3^- that formed complexes with the dyes. The slope of the fluorescence intensity of the MK-2 solution was larger than that of the MKZ-35 solution, indicating that the I_3^- concentration near MK-2 was more concentrated by the dispersion force.

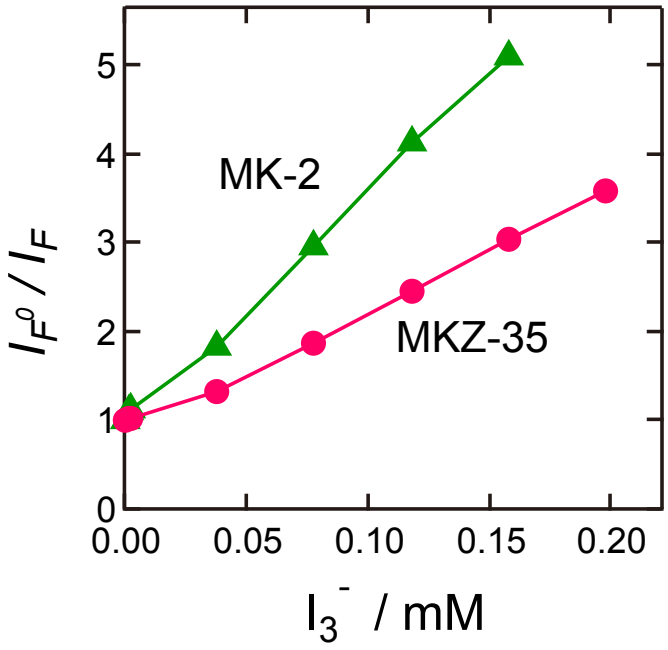

Figure 6-4. Fluorescence quenching experiments of MK-2 and MKZ-35 as a function of quencher concentration. The vertical axis is the ratio of fluorescence intensity (I_F^0/I_F). I_F^0 and I_F are the fluorescence intensities without and with a fluorescence quencher, respectively. I_3^- was chosen as a quencher and prepared by blending TBAI and I_2 at an equal ratio. The dyes were dissolved in mixed solvent (t-BuOH/AN/ toluene = 1:1:1 volume ratio).

iv. Computational chemistry experiment

The dispersion force of MKZ-35 was indicated to be smaller than that of MK-2. To explain this mechanism, I proposed a hypothesis that the dispersion force of dyes was canceled by the interaction between dyes, and the force of the interaction of MKZ-35 was stronger than that of MK-2. The dispersion force is derived from the induced dipole moment of the dye. If the dyes were located close to each other, the induced dipoles could cancel each other. This is because when a dye has an induced dipole moment, a neighbor dye also develops an induced dipole moment with the reverse vector. If the dyes interacted with each other in the dye solution, the dyes were probably adsorbed closely on TiO_2. Here, to estimate the interaction force between dyes, a computational chemistry experiment was employed. The semi-empirical molecular orbital method of MOPAC AM1 level calculation indicates that the MKZ-35 molecules were attracted to each other. This indicates that the interaction of canceling the induced dipole moments between dyes reduces the I_3^- concentration near the semiconductor electrode surface.

6-1-4. Conclusions

When the non π-conjugated moiety was added to the anchor unit of the D-π-A type organic dye, the I_{sc} was decreased, and the V_{oc} was increased. The I_{sc} decreasing was caused by decreasing the injection efficiency from the excited state dye to TiO_2. The higher V_{oc} of the DSSCs with MKZ-35 was caused by the longer electron lifetime. This longer electron lifetime

was derived from the interaction between dyes. This interaction reduced the dispersion force of the dye layer on TiO_2 surface. As a reuslt, the I_3^- concentration near semiconductor surface was decreased. Therefore, not only the blocking effect but also reducing dispersion force is effective approach to obtain longer electron lifetime. It was indicated that the dispersion forces were decreased with cancel of the induced dipole moment between each dyes. To cancel induced dipole moment, condition of dye in the solution should be taken into account. This is because the dispersion force was reproduced the condition in the solution on the TiO2 surface as well.

6-2. References

1 M. Miyashita, K. Sunahara, T. Nishikawa, Y. Uemura, N. Koumura, K. Hara, A. Mori, T. Abe, E. Suzuki, S. Mori, *J. Am. Chem. Soc.*, 2008, **130**, 17874-17881.

2 N. Koumura, Z.-S. Wang, S. Mori, M. Miyashita, E. Suzuki, K. Hara, *J. Am. Chem. Soc.*, 2006, **128**, 14256-14257.

3 A. Hagfeldt, G. Boschloo, L. Sun, L. Kloo, H. Pettersson, *Chem. Rev.*, 2010, **110**, 6595-9993.

4 A. Yella, H.-W. Lee, H. N. Tsao, C. Yi, A. K. Chandiran, M. K. Nazeeruddin, E. W.-G. Diau, C.-Y. Yeh, S. M. Zakeeruddin, M. Grätzel, *Science*, 2011, **334**, 329-634.

5 S. Mathew, A. Yella, P. Gao, R. Humphry-Baker, B. F. E. Curchod, N. Ashari-Astani, I. Tavernelli, U. Rothlisberger, M. K. Nazeeruddin, M. Grätzel, *Nature Chemistry*, 2014, **6**, 242-247.

6 G. Zhang, H. Bala, Y. Cheng, D. Shi, X. Lv, Q. Yu, and P. Wang, *Chem. Commun.*, 2009, 2198–2200.

7 W. Zeng, Y. Cao, Y. Bai, Y. Wang, and Y. Shi, *Chem. Mater.*, 2010, **22**, 1915–1925.

8 T. Uchiyama, T. N. Murakami, N. Yoshii, Y. Uemura, N. Koumura, N. Masaki, M. Kimura, S. Mori, *Chem. Lett.*, 2013, **42**, 453-454.

9 D. Joly, L. Pelleja, S. Narbey, F. Oswald, J. Chiron, J. N. Clifford, E. Palomares, and R. Demadrille, *Scientific Reports*, 2014, **4**, 1–7.

10 H. Inoue, K. Takagi, M. Sasaki, and C. Pac, 1990, "Hikarikagaku I (Photochemistry I)", Maruzen Publishing, ISBN978-621-04656-2, Printed in Japan.

11 K. E. Splan, A. M. Massari, and J. T. Hupp, *J. Phys. Chem. C*, 2004, **108**, 4111–4115.

Chapter 7

Conclusions

Chapter 7. Conclusions

In this thesis, I studied the determination factors of the electron transfer kinetics in dye-sensitized solar cells (DSSCs). This was motivated to obtain design guides of molecular structure of the dyes to improve the power conversion efficiency. I focused on the reduction kinetics of the dye cation generated by electron injection and the electron lifetime in the semiconductor electrode, and I evaluated the effects of molecular structure differences in the dye on the kinetics.

In chapter 1, I introduced the history, the background of DSSCs, and the aim of the studies.

In chapter 2, I explained the fabrication procedures and characterization methods of the DSSCs. I showed that the dye cations absorbed near-infrared light and reduction rate of dye cation related to half time of transient absorption decay in the near-infrared region.

In chapter 3 and 4, I examined the structure effects of donor, π-conjugated linker and acceptor (D-π-A) type organic dyes on the reduction kinetics of dye cations.

In chapter 3, I examined donor structure effects of D-π-A type organic dyes on the reduction kinetics. I found that a dye with large surface area of accessible HOMO can obtain

high regeneration efficiency in DSSCs. The effect of the accessible HOMO area on the regeneration rate was lager than the effect of the around 200 meV energy difference between the HOMO of dye and the redox potential. The regeneration rate was also accelerated by reducing the adsorption density of the dyes on the surface of TiO_2 electrode. On the other hand, the recombination rate was not changed by the donor structure difference at low electron density in the TiO_2 electrode.

In the chapter 4, I demonstrated that the introduction of alkyl chains to the π-conjugated linker decelerated the regeneration rate and the recombination rete. The alkyl chains decreased the electronic coupling between the HOMO of the dye and I^-. Therefore, the regeneration rate was decelerated. I showed that the recombination rate was accelerated by hole hopping between adsorbed dyes. The introduction of alkyl chains prevented the hole hopping between dyes. Thus, the recombination rate was decelerated.

The design guides to obtain DSSCs with high regeneration efficiency are described below;

(1) Employ sterically-bulky donor unit for fast regeneration rate of dye cations: The faster regeneration rate will be obtained by large accessible area of HOMO to I^- in the electrolyte.
(2) Introduction of obstacle units: The obstacle units can prevent an approach of I_3^- in electrolytes to TiO_2 surface and the hole hopping between dyes, and then the electron lifetime will increase.
(3) The electronic coupling between HOMO of dye and I^- should not be decreased by the obstacle units.

In chapters 5 and 6, I evaluated the electron lifetime in a semiconductor electrode.

In chapter 5, I examined the required conditions for an electron lifetime measurement system and developed a new electron lifetime measurement system. The stepped light-induced transient measurements of photocurrent and voltage (SLIM-PCV) method requires uniform excitation of dyes in the photo-electrode. I clarified that the absorbance of photo-electrode should be less than 1 for diffusion coefficient measurement. On the other hand, I clarified that the absorbance of the photo-electrode should be less than 3 for the electron lifetime measurement. I developed a stepped current induced measurement of cell voltage in the dark (darkSCIM) method. The darkSCIM method uses a galvanostat for electron injection into the semiconductor electrode. An electron injection system of this method is different from the SLIM-PCV method, which uses light irradiation. To measure the electron lifetime of the new system, the injected electron current was stepped and the transient voltage decay was simultaneously measured. The electron lifetimes can be obtained by fitting the transient voltage response to an exponential function. The electron lifetime measured by the darkSCIM method was consistent with the electron lifetime measured by the SLIM-PCV method. Therefore, the validity of the darkSCIM method was demonstrated.

In chapter 6, I clarified that the electron lifetime was improved by the suppression of the dispersion force by interaction of the dye molecules in DSSCs using organic dyes. The dispersion force is formed by induced dipole moment. The dipole moment attracts I_3^- in the

electrolyte close to TiO_2 surface, and then the concentration of I_3^- near TiO_2 surface becomes higher. Therefore, the electron lifetime is decreased. I showed the interaction between dyes canceled the induced dipole moment.

Publications and participation in conferences

List of Publications

Junichi Ogawa, Nagatoshi Koumura, Kohjiro Hara, and Shogo Mori

"Deceleration of dye cation reduction kinetics by adding alkyl chains to the π-conjugated linker of dye molecules"

Japanese Journal of Applied Physics, 53 (Submitted)

Junichi Ogawa, Satoshi Nishikawa, Toshikazu Hasegawa, and Shogo Mori

"Required Conditions for SLIM-PCV Methods to Measure Electron Diffusion Coefficients and Lifetime in Dye-Sensitized Solar Cells"

Electrochemistry, 80 (2012) 886-890

Kenji Sunahara, Junichi Ogawa, and Shogo Mori

"A method to measure electron lifetime in dye-sensitized solar cells: Stepped current induced measurement of cell voltage in the dark"

Electrochemistry Communications 13 (2011) 1420-1422

Xue-Hua Zhang, Junichi Ogawa, Kenji Sunahara, Yan Cui, Yu Uemura, Tsutomu Miyasaka, Akihiro Furube, Nagatoshi Koumura, Kohjiro Hara, and Shogo Mori

"Alternation of Charge Injection and Recombination in Dye-Sensitized Solar Cells by the Addition of Nonconjugated Bridge to Organic Dyes"

The Journal of Physical Chemistry C, 117 (2013) 2024-2031

International conferences

Junichi Ogawa, and Shogo Mori

"Charge recombination in dye-sensitized solar cell: Influence of dye cation and free energy difference"

18th International Conference on Photochemical Conversion and Storage of Solar Energy, P1-31, Seoul, Korea (July 2010)

Junichi Ogawa, Kazumichi Obuchi, Nagatoshi Koumura, Mutsumi Kimura, and Shogo Mori

"Influences of Electrolyte and Dye structure on the Reduction Rate of Dye Cation in Dye-Sensitized Solar Cells"

The 6th Aceanian Conference on Dye-sensitized and Organic Solar Cells, P077, Beppu, Oita, Japan (October 2011)

Junichi Ogawa, Nagatoshi Koumura, Mutsumi Kimura, and Shogo Mori

"Effect of dye structure on the reduction rate of dye cation in dye-sensitized solar cells"

Hybrid and Organic Photovoltaics Conference, Uppsala, Sweden (May 2012)

Junichi Ogawa, Nagatoshi Koumura, Mutsumi Kimura, and Shogo Mori

"Effect of alkyl chains on the regeneration rate of dye cation in dye-sensitized solar cells"

Hybrid and Organic Photovoltaics Conference, P100, Sevilla, Spain, (May 2013)

National conferences

Junichi Ogawa, Kenji Sunahara, and Shogo Mori

"A method to measure electron lifetime in the dark for Dye Sensitized Solar Cells"

The Electrochemical Society of Japan, 78th meeting, 3G05, Yokohama, March 2011

Junichi Ogawa, Kazumichi Obuchi, Nagatoshi Koumura, Mutsumi Kimura, and Shogo Mori

"Influences of electrolyte and dye structure on the reduction rate of dye cation in dye sensitized solar cells"

The Electrochemical Society of Japan, autumn meeting, 2N03, Niigata, September 2011

Junichi Ogawa, Nagatoshi Koumura, Yu Uemura, Kohjiro Hara, and Shogo Mori

"Influences of partial charge in molecule on the reduction rate of dye cation in dye sensitized solar cells"

The Electrochemical Society of Japan, 79th meeting, 2O05, Hamamatsu, March 2012

Junichi Ogawa, Nagatoshi Koumura, and Shogo Mori

"The relation between reduction rate of dye-cation and dye molecular structure on dye-sensitized solar cells"

The Electrochemical Society of Japan, 81th meeting, 2M03, Osaka, March 2014

Acknowledgements

My deepest appreciation goes to Associate Professor Shogo Mori for the continued support and guidance during my academic life. I have learned several experimental techniques and scientific thinking from him. I am also grateful to him for allowing me to attend conferences and study overseas at the Wollongong University in Australia and the Jaume I University in Spain.

I would like to thank Professor Mutsumi Kimura for scientific advices, support and encouragement. I have studied fundamentals of material synthesis. I would sincerely appreciate the provision of the dyes from Dr. Nagatoshi Koumura. Completion of my experiments would not have been possible without the cooperation from Koumura-San's group.

I am also grateful of Dr. Masaki Naruhiko for his experimental advice and kind support. Furthermore, I would like to express my gratitude to Dr. Takurou N. Murakami, Dr. Takahiro Kono, Dr. Sunahara Kenji, Dr. Yu Uemura, and Dr. Saurabh Agrawal for exciting discussions, valuable suggestions, support, and encouragement.

I appreciate the valuable discussion and precious experience received from Dr. Attila J. Mozer, Dr. Pawel Wagner, Mr. Long Zhao and Intelligent Polymer Research Institute members at Wollongong University, Australia.

On the overseas education at the Jaume I University, I appreciate the valuable discussion and precious experience received from Professor Juan Bisquert Mascarell, Professor Germà Garcia-Belmonte, Dr. Antonio Guerrero Castillejo and Photovoltaic and Optoelectronic Devices Group members.

During the PhD student life, Mr. Keisuke Takemoto, Mr. Koichi Okuda, Kimura group members, and Mori group members give me exciting days and warm encouragement. I would like to use this space to sincerely thank all friends from the bottom of my heart.

These studies were partially supported by Grants for Excellent Graduate Schools, MEXT, Japan and New Energy and Industrial Technology Development Organization (NEDO) of Japan.

Finally, I would like to express my gratitude to my family for their financial support and great affection.

Junichi Ogawa

March 2015.